
Radio Studies of Solar-Terrestrial Relationships



LOIS Science Team

Edited by Bo Thidé

March 18, 2002

Contents

Summary	3
1 Introduction	5
2 Remote Sensing of Geospace and the Inner Heliosphere	6
3 Solar Radar	8
3.1 Fundamental Solar Atmospheric Research	12
3.1.1 Ray Trace Modelling of Solar Radar Experiments	17
3.2 Applied Solar Atmospheric Research—“Space Weather”	20
3.2.1 The Morphology of Coronal Mass Ejections	21
3.2.2 CME Probing at Frequencies Outside the Optical Range	23
3.2.3 Monitoring CMEs from the Ground	23
4 Solar Wind Radar	26
5 High-Altitude Magnetospheric Radar	28
6 Low-Altitude Magnetospheric Radar	29
7 General Remarks	29
7.1 Solar Observations	30
7.2 Magnetospheric Scatter	31
7.3 Radar Scattering Centres of Consequence to Deep-Space Probing	31
8 Siting Options	32
8.1 Australia	33
8.2 North America	33
8.3 Europe	34
8.3.1 Case Study 1: Collaborative Magnetospheric Observations using LOFAR-LOIS and the EISCAT Incoherent Scatter Radars	34
8.3.2 Case Study 2: Collaborative Studies between LOFAR-LOIS and the EISCAT High-Power HF Transmitter	35
8.4 Bistatic Radar Geometry	36
References	41

Contributors

HENRY AURASS	API, Potsdam, Germany
YURIY BELOV	NIRFI, Nizhniy Novgorod, Russia
ARNOLD BENZ	ETH, Zürich, Switzerland
NATALY BLAGOVESHCHENSKAYA	AARI, St. Petersburg, Russia
BENGT ELIASSON	IRF/Uppsala University, Sweden
VLADIMIR FROLOV	NIRFI, Nizhniy Novgorod, Russia
SAVELIY GRACH	NIRFI, Nizhniy Novgorod, Russia
CHRISTIAN HANUISE	LPCE/CNRS, Orléans, France
BRETT ISHAM	EISCAT, Tromsø, Norway
ALEXANDER KONOVALENKO	IRA, Kharkov, Ukraine
THOMAS LEYSER	IRF, Uppsala, Sweden
HENRIK LUNDSTEDT	IRF, Lund, Sweden
GOTTFRIED MANN	API, Potsdam, Germany
PETER ROBINSON	University of Sydney, Australia
FRANCIS SEDGEMORE	DSRI, Copenhagen, Denmark
OLGA SHEINER	NIRFI, Nizhniy Novgorod, Russia
MICHAEL STARKS	AFRL, Bedford, MA, USA
KRISTOF STASIEWICZ	IRF, Uppsala, Sweden
ÅKE STEEN	RemSpace Group, Linköping, Sweden
BO THIDÉ	IRF, Uppsala, Sweden
YURIY TOKAREV	NIRFI, Nizhniy Novgorod, Russia
ANDERS VÄSTBERG	RIT, Stockholm, Sweden
JÜRGEN WATERMANN	DMI, Copenhagen, Denmark

Summary

The solar corona can be probed using ground-based radar operating in the 10–100 MHz frequency range. This has been demonstrated via radar observations performed during the second half of the past century, which were however impeded by low sensitivity and coarse resolution, leaving the puzzling complexity of the signals largely unresolved. This is also supported by modern ray tracing simulations using numerical models of the solar corona. By now, our understanding of the structure and dynamics of the solar atmosphere is much more advanced so that a new attempt to probe the solar corona with a powerful and sophisticated radar facility appears to be a timely research project.

The high frequency (HF, 3 to 30 MHz) and very high frequency (VHF, 30 to 300 MHz) radar bands provide for a sensible complement to the visible regime and are expected to yield a quantitative description of plasma density, velocity and turbulence at different altitudes within the solar atmosphere. Of scientific interest are the structure of the corona under quiet conditions (ground state) as well as at various levels of activity. Of particular interest to us are the most active regions because they exert a major influence on geospace with potentially grave effects in the human environment. The most prominent manifestations of the active Sun include coronal mass ejections (CMEs), solar flares, and low-latitude coronal holes (regions of open magnetic field lines and high velocity solar wind).

These regions are sources of “adverse space weather”, *i.e.*, conditions in geospace which adversely affect human health and operations of technological systems. It is therefore of great importance to human society to monitor the development and propagation of energetic solar events. An operational space weather program, *i.e.*, one capable of routine observation and forecast, must build on fundamental space and atmospheric research. Space weather research aims to understand the physics governing solar activity and its consequences and helps to build and subsequently improve dynamic models. An integrated receiver-transmitter system based on the LOFAR facility but augmented with an external radar sub-facility will form an important element in space weather research.

The ability to physically utilise and computationally model the orthogonal O and X mode radio wave polarizations separately has important implications for the monitoring of the corona, as the different polarisations have distinct magnetic characteristics, which might in principle be used to measure and monitor the coronal magnetic field.

The deeper worth of the radar extension is found in the valuable contribution that ground-based radar measurements of coronal turbulence and magnetic fields can make to our modern network of ground- and space-based solar observatories. Solar radar observations are expected to provide important and unique complementary information that will assist in the interpretation of other measurements, thus allowing the more accurate forecasting of space weather events.

1 Introduction

To study the fundamental physical principles governing the Earth's space environment and thereby better understand and, more importantly, predict the effect of solar-terrestrial processes which define the conditions for life on and around our own planet, powerful and sophisticated instruments are required. Observations from spacecraft moving with speeds of several kilometres per second typically provide snapshots from this environment and are ideally combined with observations of processes taking place on large spatial scales and over extended time periods as provided by ground-based space research facilities. Furthermore, many regions of solar-terrestrial space can only be probed by instruments which sense the processes remotely. An example of such a region is the inner solar atmosphere.

A judiciously designed radio facility such as the Low Frequency Array (LOFAR) radio telescope¹ is versatile and flexible enough to allow the passive study of a large variety of physical phenomena in virtually all space regions of central interest for present and future space physics, from the Earth's neutral atmosphere to the Sun and even beyond, with one and the same instrument. Realising that it would be difficult to motivate scientifically, politically, and financially, the construction of a relatively costly, specialised, essentially single-purpose large research instrument, the LOFAR facility has the attractive feature of being able to operate as a multi-purpose radio observatory of a new kind for use in ground-based space physics, astrophysics and environmental research.

Here, we propose that the receive-only LOFAR radio telescope be augmented by a ground-based transmitter/radar facility which enables deep-space HF/VHF radar applications and advocate first and foremost radar probing of the solar atmosphere. The addition of radar capability to LOFAR will not lead to any major new or costly technical requirements in the strawman LOFAR design. Furthermore, the groups responsible for the radar-specific facilities and infrastructure will ensure proper development in that area.

Since the pioneering radio experiments of the early 20th century, many active radio and radar techniques have been developed for the study of the near-Earth space. The literature describing this development and the employment of the various techniques is plentiful (*e.g.*, *Davies* [23], *Hunsucker* [49], and *Kohl et al.* [62]).

Space radar techniques can be uniquely powerful methods of obtaining information not only on near-Earth space but also on planetary objects including planets, moons, asteroids, and comets; the interplanetary medium; and the Sun. Measurements of the distribution of echo power versus direction angle (image), time delay (range), Doppler frequency (radial velocity), spectral width (turbulence), and radio wave polarisation (magnetic field) constitute multi-dimensional observations of potentially high resolution, given high enough signal-to-noise ratios.

A key factor in space radar investigations is human control of the transmitted signal used to illuminate the target. While virtually every other astronomical

¹<http://www.lofar.org>

technique relies on passive measurement of reflected sunlight or naturally emitted radiation, radar uses coherent illumination whose time/frequency/phase structure and polarisation state are designed by the scientist. The general stratagem of a radar observation is to transmit a signal with well-defined characteristics and then, by comparing the echo to the transmission, deduce the target's properties. Hence, the observer is intimately involved in an active observation and, in a very real sense, performs a controlled experiment on the target.

Deep-space radar studies are made possible through the utilisation of highly sensitive antennas and receivers along with radio transmitters powerful enough for the study of our space environment well beyond the ionosphere and the lower magnetosphere, which have been the targets for existing traditional scatter radars. Such observations are performed by the Arecibo radar in Puerto Rico and the Goldstone radar in California. The bulk of the deep-space radar investigations performed to date have been studies of hard target bodies at very short radar wavelengths, typically at S band and X band frequencies [82].

However, the advent of efficient digital techniques for system control and data handling now allows for the flexible, cost-effective design of large, long-wavelength (HF/VHF) transmitting and receiving antenna arrays. Thus, we now have the ability to build long-wavelength radar facilities which can perform radar studies with a sensitivity and sophistication that has not been previously possible, thereby opening a new frequency window in active deep-space radio research.

2 Remote Sensing of Geospace and the Inner Heliosphere

The inner heliosphere is usually defined as the part of the circumsolar region where the solar magnetic field deviates 45 degrees or less from the radial direction. This corresponds roughly to radial distances out to one astronomical unit ($1 \text{ AU} = 1.496 \times 10^{11} \text{ m}$) and encompasses the sunward part of geospace.

While processes in the inner heliosphere and geospace are of decisive importance for Earth's interplay with its space surrounding and for life on Earth itself, many of these processes are still not well understood.

In order to overcome these shortcomings in our present knowledge, we propose that the LOFAR radio telescope, operated in the 10–240 MHz frequency range (30–1.25 m vacuum wavelength range), be augmented by a sub-facility for transmission and reception in the same frequency (wavelength) range. This would allow for the remote radar probing, from the ground, of these regions of space with an unprecedented sensitivity and versatility.

In situ measurements of the interplanetary medium in the near-solar environment at about $0.3 \text{ AU} = 62R_{\odot}$ ($1R_{\odot} = 6.96 \times 10^8 \text{ m} = 109 \text{ Earth radii}$) were performed in the *Helios* missions [96] but measurements of the regions much closer to the Sun have to be made with remote sensing techniques. Spacecraft with approaches down to $45R_{\odot}$ or closer (*e.g.*, *Solar Probe* and *Solar Orbiter* [75]) have

been planned but cancelled, or will, according to recent ESA decisions, not be built until 2013.

In addition to solar radar, remote sensing techniques which have been used to date for studies of the Sun inside of 0.3 AU include

1. The analysis of radio emissions generated naturally within the region and observed on Earth or on spacecraft. The proposed *Frequency Agile Solar Radiotelescope (FASR)*,² possibly to be sited near the Owens Valley Radio Observatory in California, is an example of a new, interesting ground-based facility for the passive observation of the Sun in the 0.1–30 GHz frequency range.
2. Diagnostics of the solar corona with radio transmission and methods utilising mainly natural radio sources but also spacecraft beacons. The diagnostics include
 - (a) Group delay observations using spacecraft, pulsar and planetary radar signals. They give good total electron content (TEC) observations.
 - (b) Phase scintillation using
 - i. Spacecraft transponders.
 - ii. Natural radio sources and interferometer receivers including multi-element radio interferometric facilities [6].
 - (c) Intensity scintillation using natural sources.
 - (d) Angular broadening using natural radio sources and receiving arrays.
 - (e) Spectral broadening of spacecraft beacons.
 - (f) Pulse broadening of pulsars.
3. Optical observations.
 - (a) UV emission lines can be detected out to about $4R_{\odot}$. These provide very useful diagnostics on temperature, velocities, turbulence, composition, flow speed, *etc.*
 - (b) Scattered white light has been detected out to $30R_{\odot}$ using traditional coronagraphs on spacecraft as for instance C3 on *SOHO*, and even further using specialised photometers such as those on *Helios*. These observations provide electron density data directly. Optical observations have become very important for coronal studies particularly since instruments were placed in orbit. *Solwind*, *Skylab ATM*, *SMM*, *Yohkoh*, *SOHO*, and *TRACE* have been responsible for most of our information on the coronal plasma. New coronagraphs and photometers will be flown on *Solar-B*, *SMEI*, and *STEREO*.

²<http://www.ovsa.njit.edu/fasr>

- (c) The *Solar Mass Ejection Imager (SMEI)*, a space-borne instrument will be launched during 2002 by the U.S. Air Force Research Laboratory. It consists of CCD cameras and baffles for detecting and measuring coronal mass ejections optically in the 450–1100 nm wavelength range [116].
- (d) The *Solar Terrestrial Relations Observatory (STEREO)* mission is planned for launch in 2005 by NASA. The aim is to make 3-dimensional studies of the Sun by using optical instruments supplemented by passive radio measurements.

4. Magnetic field measurements.

The magnetic field in the corona can be measured via Faraday rotation of radio signals passing through it [4, 72], but the mean field cancels out and one can only measure fluctuations in the product BN_e . This is a serious problem because the magnetic field is considered to be a prime source of energy for heating the corona and accelerating the solar wind. Solar radar can measure the radial component of the magnetic field directly using the differential delay between X and O modes, but this was not done in earlier experiments because they used linear polarised receivers. In UV light, one can exploit resonant line scattering polarisation measurements to diagnose the magnetic field (the Hanle effect [43]). For strong fields, the Zeeman effect can be used.

A combination of one or several of the above techniques and solar radar, which will be described next, will allow a two-phase approach where the objective of phase one will be to establish the solar radar as an useful and unique diagnostic tool. Phase two, where the radar is used more or less as a space counterpart of the common weather radars for making predictions and forecasts of the space weather, would then be the next logical step.

3 Solar Radar

Kindled by the discoveries by *Hey* and *Southworth* in the early 1940s [44, 103] that the Sun emits radio waves at metre and centimetre wavelengths, systematic studies of the solar environment with radio methods have by now been carried out for five 11-year solar cycles [64]. In 1952 *Kerr* [60] proposed that radar studies of the Sun could be performed. Further considerations of the solar radar concept were made a few years later by *Bass and Braude* [8] and *Kerr* [61].

However, the solar atmosphere absorbs some of the radar signal intensity according to the well-known optical depth formula $I(\omega) = I_0 \times \exp[-\int \kappa(\omega) dz]$, where κ is the absorption index and $\kappa(\omega)$ is principally determined by the solar atmospheric density and temperature profiles and is found to exhibit a ω^2 dependence. This limits the frequency range for a solar radar to below 100 MHz or so.

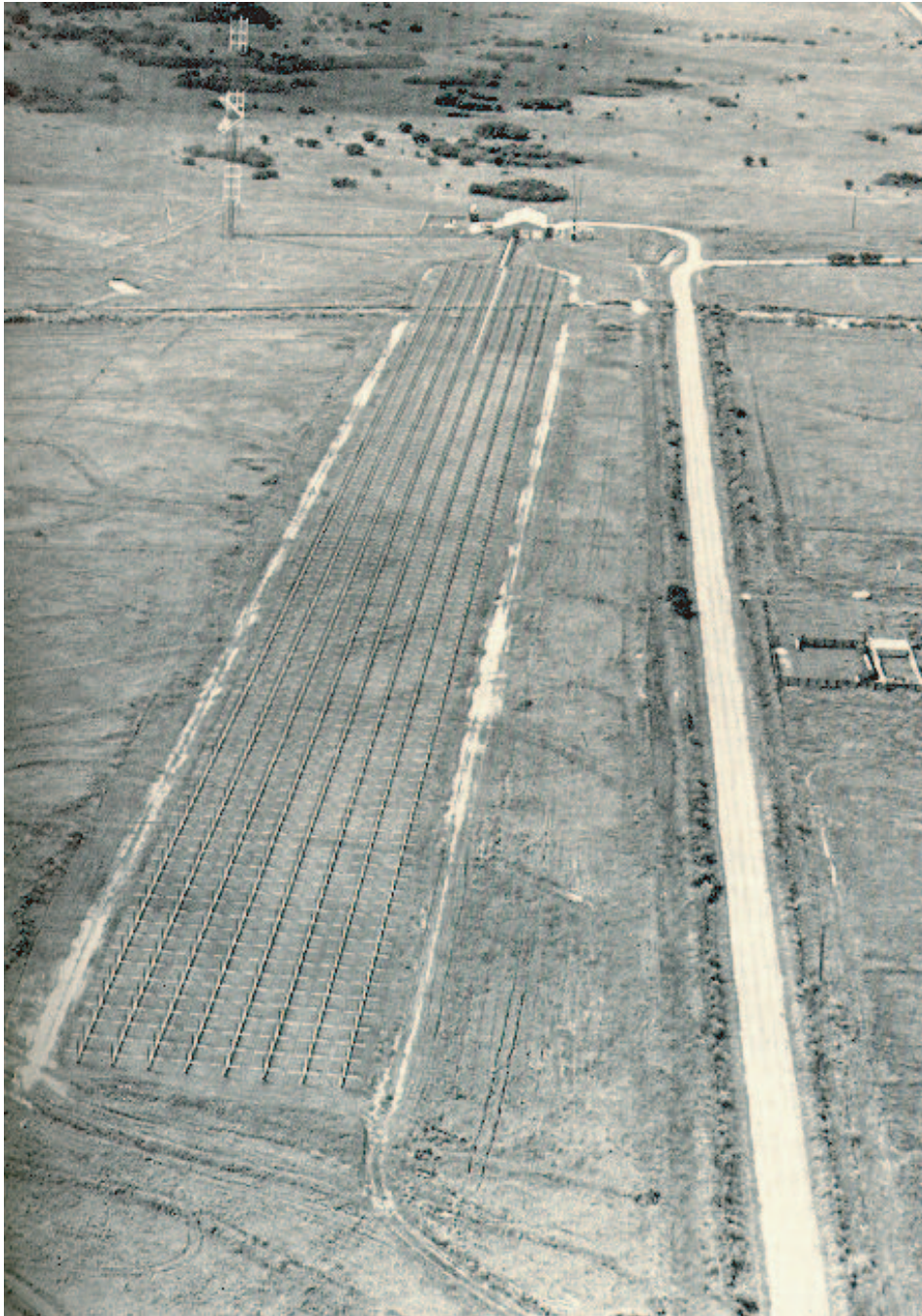


FIGURE 1: The El Campo, TX, radar as used by *James* in the 1960s.

SOLAR RADAR PHYSICS

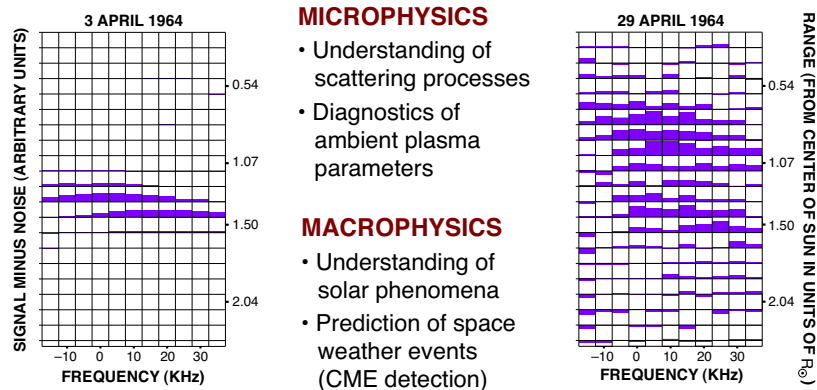


FIGURE 2: A solar radar can give information on the local physics in the solar atmosphere. The two data panels left and right are actual results from the El Campo radar.

The main constraint on the lowest usable frequency is set by the ionosphere. It is transparent for frequencies of the order 5–10 MHz and higher, depending on the site, time of the day and time of the year. But even for frequencies above this cut-off, corrections for the ionospheric distortions on both the transmitted and received radar signals must be made with self-calibration techniques or similar.

Direct probing of the solar atmosphere with radar techniques have been performed by a number of workers:

1. In 1959, *Eshleman et al.*, in California, detected the corona at 25.6 MHz, at a time when the coronal radar cross section was greatly enhanced over the average level [30]. The point of reflection was determined at 1.7 photospheric radii from the centre of the Sun.
2. From 1961 to 1969 *James* made a single daily observation of the corona at local noon, using a much more powerful 38.25-MHz radar system at El Campo in Texas, [51, 53, 54, 55]. The echoes were typically blue-shifted.
3. In the mid-1960s, *Campbell and Parrish* detected the corona using a 40-MHz transmitter at Arecibo with much lower effective radiated power (ERP) than the El Campo radar [84, 20]. They confirmed *James*' results but were severely limited by the low sensitivity of the 40-MHz Arecibo system.
4. In 1977 and 1978 *Benz and Fitze* attempted to observe scatter from Langmuir waves in the corona using a 2.6 GHz, 500 MW CW transmitter at Arecibo [12, 13, 31] but were not successful, most likely because of the very high frequency used.

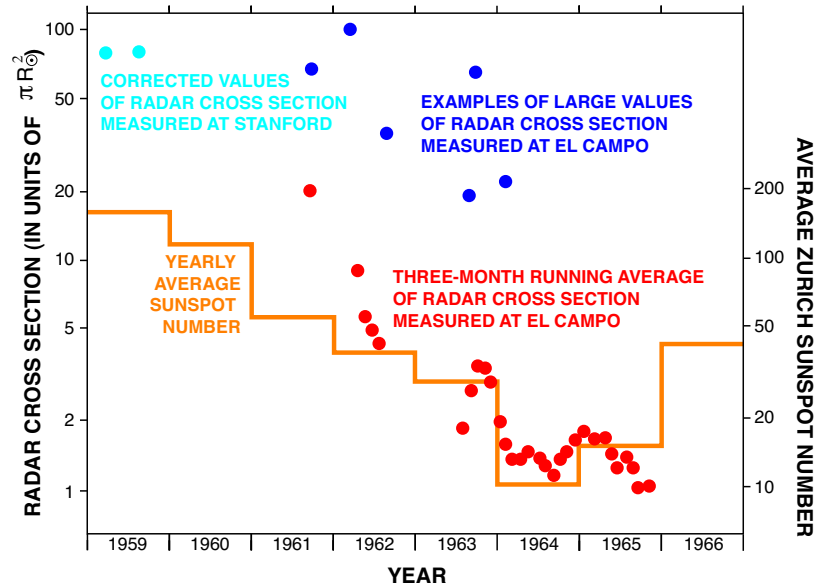


FIGURE 3: Radar cross section of the Sun as measured by *James* at 38.25 MHz.

5. From 1996 to 1998 solar radar experiments were carried out at 9 MHz using the Russian Sura high-power radio transmitter together with the Ukrainian UTR-2 radio telescope in a bistatic mode [94, 93], and there was a likely marginal detection of the corona with a Doppler bandwidth of about 40 kHz. During this period Sura was also used in a monostatic mode at 9 MHz [59, 58]; the analysis of the monostatic data is currently in progress [57].

The El Campo radar, built by MIT's Lincoln Laboratory and pictured in Figure 1, detected 38.25-MHz radar echoes from the Sun for a period of nine years in the 1960s [1, 2, 52]. Huge, rapidly-moving targets were occasionally observed, but this was before the space-borne coronagraph discovery of coronal mass ejections (CMEs), and the physical nature of these radar targets was a mystery [21]. It has been proposed that radar echoes from CMEs were being detected [92].

Hence, *James*' 1960s results, illustrated by Figures 2 and 3, were dramatic but complex and difficult to resolve at the time. Despite its tremendous potential, solar radar is therefore still an essentially unexplored diagnostic technique. Factors which were not available to *James* and which are a strong motivation for reopening the field of fundamental solar radar research at this point in time are

- Correlative observations from *Solar and Heliospheric Observatory (SOHO)*, *Transition Region and Coronal Explorer (TRACE)*, *WIND*, *Ulysses*, and other existing or upcoming spacecraft, as well as modern ground-based solar observatories.
- Modern polarimetric techniques.

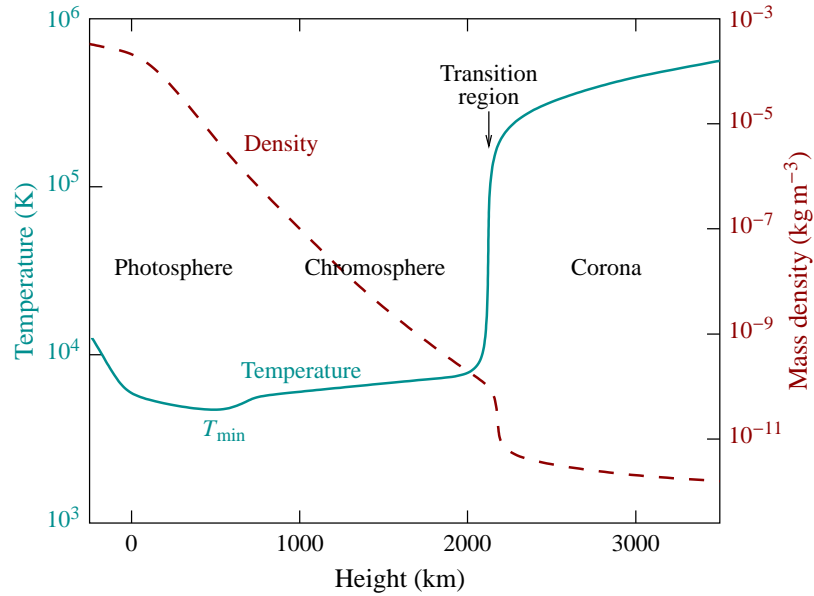


FIGURE 4: Sketch of the temperature and gas mass density in the solar photosphere, chromosphere, and lower corona, including the transition region. Adapted from *Lang* [66].

- Multi-frequency, multi-polarisation radar technologies.
- An improved general knowledge of the corona.
- Dramatically improved modelling and computing ability.

On the applied side, reliable detection and monitoring of CMEs is of great practical importance. CMEs that impact the Earth's magnetosphere can result in hundreds of millions of dollars in damage to spacecraft, communications, and electrical power systems [25]. A system of powerful, flexible low-frequency transmitters operated in software, coupled with a high-angular-resolution receiving array, would form a cost-effective system to detect and track CMEs. The rich information inherent in this measurement could open an entirely new window on CME studies, yielding their angular distribution, ranges, and line-of-sight velocities. Here we present a study of the feasibility of performing such radar studies, starting with what we know about the solar atmosphere and CMEs.

3.1 Fundamental Solar Atmospheric Research

As illustrated in Figure 4, the solar atmosphere consists of three regions:

1. The photosphere, the about 300-km-thin layer which is the main source of the Sun's optical radiation.

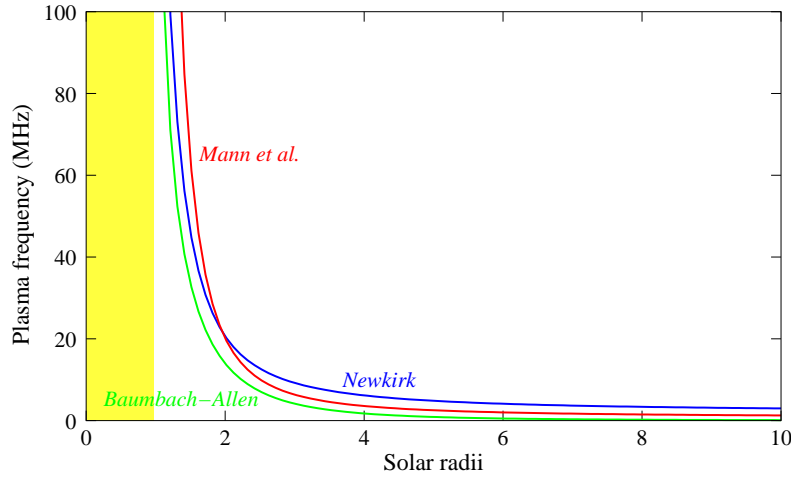


FIGURE 5: The radially dependent plasma frequency of the solar corona at a temperature of 1.0×10^6 K according to the models of *Mann et al.*, Eq. (2), red curve; *Baumbach-Allen*, Eq (3), green curve; and *Newkirk*, Eq. (4), blue curve. The yellow strip covers $1R_{\odot}$.

2. The chromosphere, a rarefied, almost completely ionised region which at a height of approximately 2×10^3 km above the photosphere changes into the corona. In H_{α} light, chromospheric structures, in the form of jets, are often clearly observed near the solar limb.
3. The corona, the extremely extensive plasma region around the Sun which can be viewed as a kind of ionosphere [34]. It consists mainly of electrons and protons and is known to absorb/emit/scatter radio radiation.

Given a powerful radar beam and a sensitive receiving array, it is possible to probe the solar atmosphere from the ground and study its properties in ways not possible with other instruments.

The electron plasma angular frequency in the solar corona can be estimated from a good model of the radially dependent electron number density $N_e(R)$ (m^{-3}) according to the well-known formula³

$$\omega_{pe}(R) = \sqrt{\frac{N_e(R)q_e^2}{\epsilon_0 m_e}} \approx 2\pi \cdot 8.98 \sqrt{N_e(R)} \quad \text{s}^{-1} \quad (1)$$

If the coronal plasma is relatively smooth and unperturbed, radar pulses will be reflected from the region where the local plasma frequency matches the radar frequency. Below we present some model calculations based on this fact.

³ q_e is the electron charge (1.60×10^{-19} C), ϵ_0 the permittivity of free space (8.85×10^{-12} F m^{-1}), and m_e the electron mass (9.10×10^{-31} kg)

TABLE 1: Electron number densities $N_{e\odot}$, critical radii R_c , and A values for three different coronal temperatures T . Adapted from [74].

T (10^6 K)	R_c/R_\odot	$N_{e\odot}$ (m^{-3})	A (m)
1.0	6.91	5.14×10^{15}	9.64×10^9
1.4	4.90	1.61×10^{14}	6.87×10^9
2.0	3.43	1.40×10^{13}	4.82×10^9

In the inner region of the corona where the flow speed v is much smaller than the critical speed $v_c = \sqrt{\kappa_B T / \mu m_p}$ attained at the critical radius $R_c = GM_\odot / (2v_c^2)$,⁴ the heliospheric density model of *Mann et al.* [74], gives the electron number density as

$$N_e(R) = N_{e\odot} \exp \left[\frac{A}{R_\odot} \left(\frac{R_\odot}{R} - 1 \right) \right] \quad (2)$$

where $A = G\mu m_p M_\odot / (\kappa_B T)$ and $N_{e\odot} = N_e(R = R_\odot)$ is the electron number density at the bottom of the corona, 2300 km above the photosphere. Actual values of $N_{e\odot}$ and A for different coronal temperatures T are given in Table 1. More sophisticated models exist, which take into account the dependence on heliographic latitude [117, 113, 14].

Other common coronal plasma density models include the semi-empirical *Baumbach-Allen* model [121, 34]

$$N_e(R) = 10^{14} \left[1.55 \left(\frac{R_\odot}{R} \right)^6 + 2.99 \left(\frac{R_\odot}{R} \right)^{16} \right] \text{ m}^{-3} \quad (3)$$

and the *Newkirk* model [81]

$$N_e(R) = 4.2 \times 10^{10} \times 10^{4.32R_\odot/R} \text{ m}^{-3} \quad (4)$$

These three models are plotted in Figure 5.

Combining the *Pätzold et al.* model, derived from *Helios* Faraday rotation measurements [90], and results from *Ulysses* measurements [86], *Mancuso and Spangler* arrive at the following model for the radial dependence of the coronal magnetic field magnitude [72]:

$$B(R) = 3.1 \left(\frac{R_{1\text{AU}}}{R} \right)^2 \text{ nT} + 0.06 \left(\frac{R_{1\text{AU}}}{R} \right)^3 \quad (5)$$

⁴ κ_B is Boltzmann's constant (1.38×10^{-23} J/K), T the coronal temperature, μ the relative mean molecular mass, assumed to have the value 0.6 [89], m_p the proton mass ($1836m_e = 1.67 \times 10^{-27}$ kg), G the gravitational constant (6.67×10^{-11} $\text{Nm}^2 \text{kg}^{-2}$), and M_\odot the solar mass (1.99×10^{30} kg).

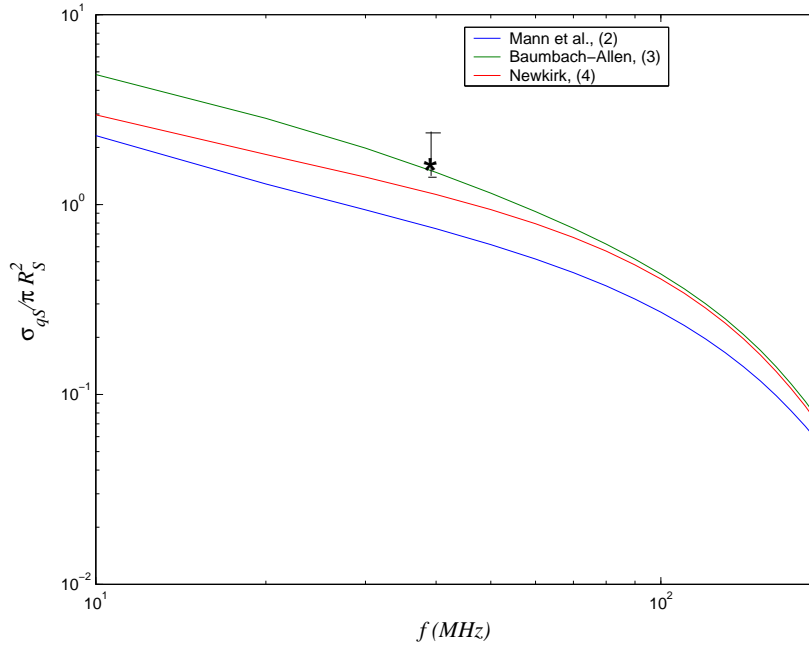


FIGURE 6: Theoretically calculated radar cross section vs. radar frequency for mirror reflection from a quiet Sun with a corona temperature $T = 2 \times 10^6$ K. The different curves correspond to different plasma density models. The black star with its error bar are the averaged value of the cross-sections in *James'* data recorded during the minimum solar activity period 1964–1965 corresponding to $1.5\pi R_\odot^2$ in Figure 3. Data provided by *Belov et al.* [11].

The effective collision frequency in the solar corona can, according to Eq. (36.5) in *Ginzburg (1970)* [34], be approximately represented by the expression

$$\nu_{\text{eff}} = \pi \frac{q_e^4}{(\kappa_B T)^2} N_e \langle \nu \rangle \ln \left(0.37 \frac{\kappa_B T}{q_e^2 N_e^{1/3}} \right) \approx \frac{5.5}{T^{3/2}} N_e \ln \left(220 \frac{T}{N_e^{1/3}} \right) \quad (6)$$

We conclude that to a good approximation the quiet solar corona can be treated as an inhomogeneous, anisotropic (birefringent), collisional plasma which is completely ionised so that any finite spatial volume consists of equal amounts of electrons and protons. We can therefore use well-established modelling methods (wave propagation theory, ray tracing, scattering analysis) to estimate the radar cross sections for a signal with a given frequency, power, beam-width, state of polarisation and direction transmitted and received by a deep-space radar on Earth. Results of such calculations are given in Figures 6 and 7.

When a significant plasma perturbation, *e.g.*, a CME, appears in the solar atmosphere, this should result in a distinct radar signature which discerns the echoes from the usual ones. We suggest that the first fundamental physics phase of the experimental investigations will be to establish such signatures. The second phase

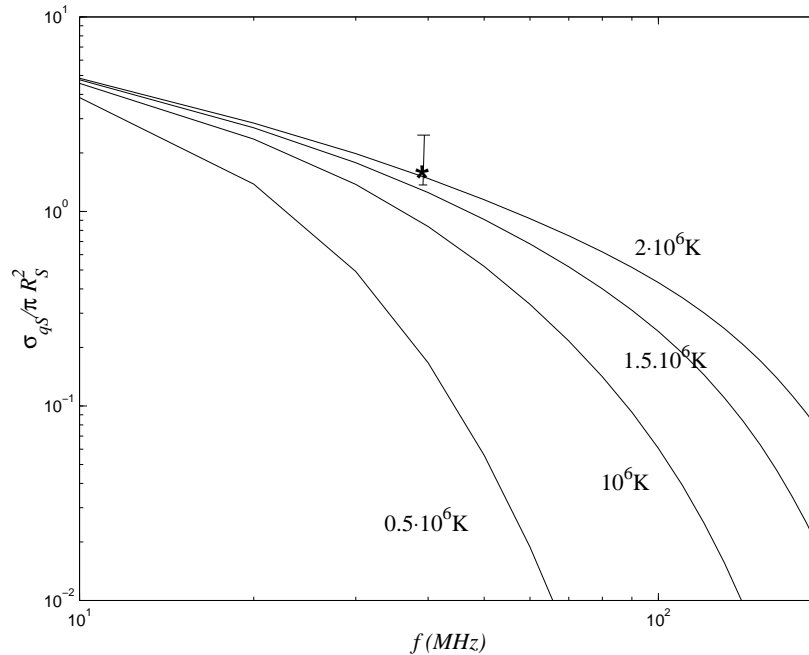


FIGURE 7: Theoretically calculated radar cross section vs. radar frequency for a quiet Sun and mirror reflection using the Baumbach-Allen electron density model (3). The different curves correspond to different corona temperatures. The black star with its error bar corresponds to the averaged value of the cross-sections in *James'* data recorded during the minimum solar activity period 1964–1965. The value equals $1.5\pi R_{\odot}^2$ in Figure 3. Data provided by *Belov et al.* [11].

will then be to perform systematic studies of the perturbations in an attempt to use the results to make predictions on their possible impact on geospace and Earth itself. Model calculations which indicate that this is feasible are presented later in this document.

The pioneering solar radar experiments in the 1950s and the 1960s revealed a complexity which, at the time, could not be attributed to specific physical processes. Adding a transmitter/radar outrigger facility to a very sensitive multi-beam telescope such as LOFAR, we would obtain an instrument with which we would be in a good position to perform basic solar research in a much better way than 30–40 years ago.

With such a new radar it will be possible to study the solar atmosphere, including the slow wind, whose origin is not yet known. An especially attractive feature is the possibility of magnetic field measurements using a combination of different transmitter polarisations and frequencies along with a full characterisation of the received echoes.

The echoes reported by *James* were often much more intense than expected, indicating that dynamic processes are at play. Wave-wave processes have been

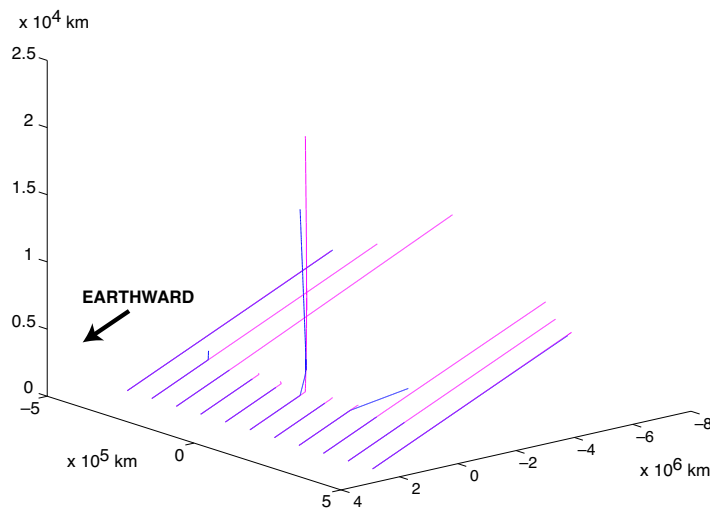


FIGURE 8: *O* mode rays approaching the Sun. Blue denotes 10 MHz, magenta denotes 38 MHz. The axes are labelled in 10^6 km, and the rays are launched $3R_{\odot}$ ($R_{\odot} = 6.96 \times 10^8$ m) on the Earthward side (positive x axis). The 38-MHz rays approach much closer to the Sun than the 10-MHz rays.

proposed in which coronal plasma waves interact with the radar waves such that an electromagnetic wave is preferentially reflected back [38, 39].

In particular, scattering from ion acoustic waves and upper hybrid waves have been suggested [12, 118]. This turbulence was predicted in the early literature at a level that may be relevant for coronal heating. It opens the possibility of probing low-frequency turbulence near the Sun where in situ measurements are not possible.

3.1.1 Ray Trace Modelling of Solar Radar Experiments

As already noted, solar radar frequencies lie between 10 and 100 MHz, in the HF (high frequency, 3–30 MHz) and VHF (very high frequency, 30–300 MHz) bands. From the measurements made in the 1960s it is known that solar radar backscatter occurs at or near the critical level in the coronal plasma, where the critical level is defined to be the point at which the EM wave frequency equals the local plasma frequency. It is well known from radio wave propagation theory and experiments that, as a ray of EM waves approaches the critical level in a magnetised plasma, it experiences strong refraction effects (Spitze effect) which cause the ray path to deviate from the “line-of-sight” path followed by waves at much higher frequencies.

Because of these strong refraction effects, modelling of the propagation of electromagnetic waves into and back out of the corona will be an essential tool required to correctly interpret radar data obtained during investigations of the near-

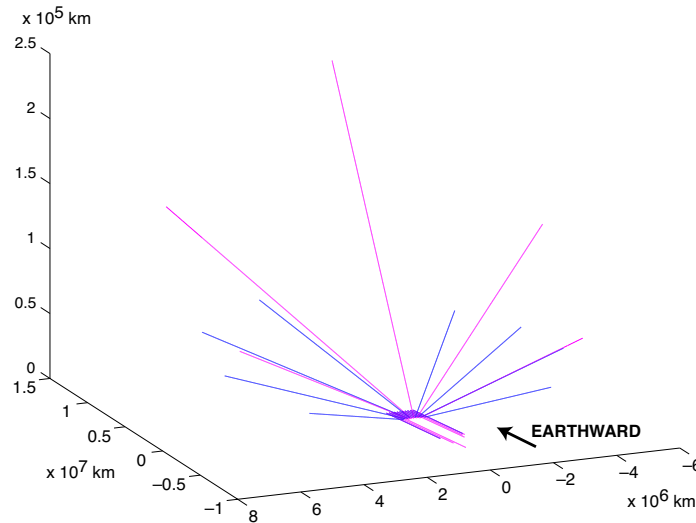


FIGURE 9: X mode rays approaching and scattering from the corona. As in Figure 8, blue denotes 10 MHz and magenta denotes 38 MHz, and the rays are launched $3R_{\odot}$ from the Sun. The viewing angle is from “behind” the Sun. Because a symmetric coronal density model was used, most rays scatter in directions away from Earth. A more realistic, irregular corona will often result in a greater percentage of incident rays which return to the receiver.

solar plasma environment. These calculations will require the use of a sophisticated 3-dimensional ray tracing code as well as the development of time-dependent models of the coronal electron density and magnetic field. During the analysis of actual measurements, we will use all available data from the international network of ground- and space-based solar observatories to generate the required models. Radar pulses will then be numerically propagated into and back from the model corona, and the results will be used to compute simulated radar data with which to compare to the observations. Undoubtedly, iteration will be required to bring the calculations into agreement with the observations, and in that way much additional information will be gained on the morphology and development of the coronal medium.

In order to demonstrate and to begin to develop this analysis capability, we have performed initial ray tracing analyses using two 3-dimensional ray tracing programs, the US Air Force Research Laboratory (AFRL) Space Weather Center of Excellence’s Power Tracing Code, and the Swedish Institute of Space Physics (IRF) ray tracing system ‘RaTS’ [114] (Figures 8, 9, 10, and 11).

The results of this analysis indicate that such investigations are indeed possible and feasible. In the AFRL test presented in Figures 8, 9, and 10, a group of ten 10-MHz and ten 38-MHz *O* and *X* mode rays were traced as they approached and traversed a spherically symmetric coronal electron density [65, 10, 5, 27] and spiral coronal **B** field [83, 48], both corresponding to ideal quiet solar conditions. The

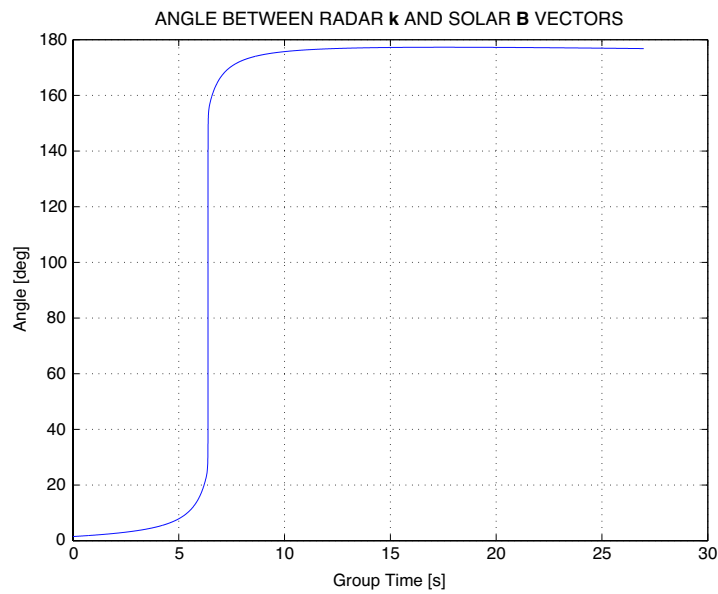


FIGURE 10: A plot showing the angle between the X mode wave \mathbf{k} vector and the local coronal magnetic field. The rays follow a field line in toward the Sun, slowly change from field-aligned to orthogonal to the field at the reflection point, then depart outward on another field line, remaining nearly field-aligned during most of their journey. Hence, these X mode rays are acting like R waves most of the time (lower left of CMA diagram).

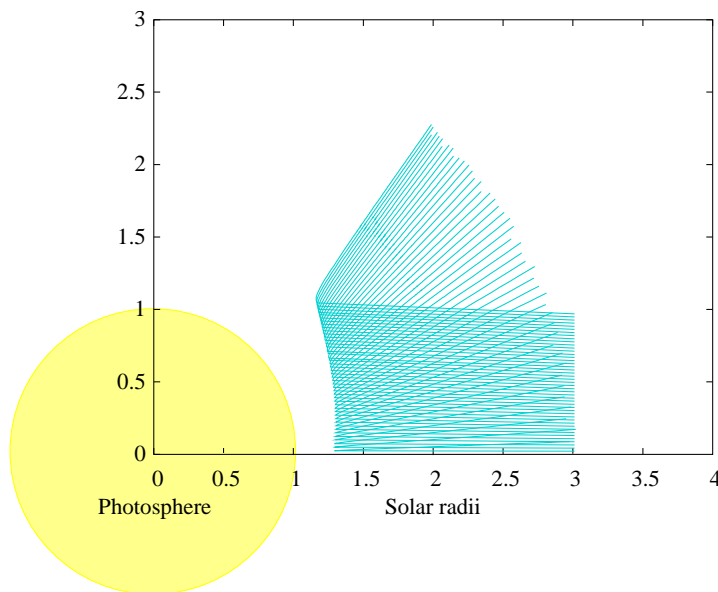


FIGURE 11: O mode rays at 38 MHz reflecting off the corona plasma. Calculated with the 'RaTS' program [114] using the *Mann et al.* model, Eq. (2).

test rays were launched in the solar equatorial plane ($z = 0$) at a distance of $x = 3R_{\odot}$ and propagated toward the Sun.

The rays were all initially parallel when approaching the Sun, oriented along the negative x axis. They were spaced $0.12R_{\odot}$ apart along the y axis, centred at $y = 0$. O mode rays approaching the Sun are shown in Figure 8. Note that the lower frequency rays scatter away from the Sun long before the higher frequency rays. This shows the advantage of multi-frequency radar observations for probing different levels within the corona. X mode rays approaching and scattering from the corona are shown in Figure 9. The spherically symmetric density model results in the great majority of the rays scattering away from the Earth. More realistic, non-symmetric and/or irregular density models will result in unpredictable variations in the backscattered signal, in agreement with the variable solar cross section observed by *James* [21, 51, 52, 53, 54, 55]. Figure 10 is a plot of the angle between the X mode wave \mathbf{k} vector and the direction of the ambient magnetic field, showing the rapid 180-degree change in direction as the rays backscatter away from the Sun. Initial results from the IRF code are similar and are presented in Figure 11.

The ability to physically utilise and computationally model X and O mode waves separately has important implications for the monitoring of the corona, as the two polarisations have different magnetic characteristics, which might in principle be used to measure and monitor the coronal \mathbf{B} field in the vicinity of the scattering region.

3.2 Applied Solar Atmospheric Research—“Space Weather”

Coronal mass ejections (CMEs) are, along with coronal holes (regions of open magnetic field lines emerging from the corona), the most geoeffective manifestations of solar activity. Geoeffectiveness means that perturbations of the near-Earth environment (geomagnetic storms) arise which are known as disturbances of the “space weather,” with the potential for manifold consequences on civilisation [101]. Geomagnetic storms associated with coronal holes tend to recur with the 27-day solar rotation while CMEs play a substantial, and possibly dominant, role in non-recurrent geomagnetic storms [76].

The ESA Space Weather Programme has set a number of goals, including identifying the measurements to be made on the ground and in space in order to provide centres with relevant data, to present a forecast prototype, and to propose a space weather centre.⁵

The US National Space Weather Program has identified CMEs as one of the most important ingredients in space weather research and monitoring [79]. However, by far not all earthward directed CMEs initiate a geomagnetic storm. There is mounting evidence that a southward oriented interplanetary magnetic field is crucial for initiating a major geomagnetic disturbance [36] and for causing variations in the critical plasma frequency of the ionosphere.

⁵<http://www.irfl.lu.se/HeliosHome/esaswprogram.html>

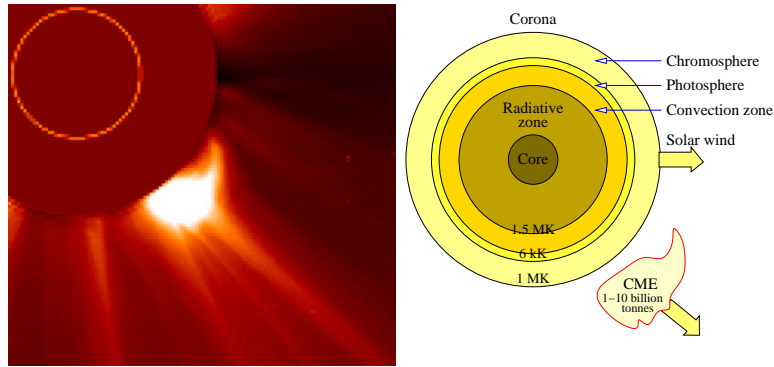


FIGURE 12: Coronal mass ejections (CMEs) have been identified in the optical frequency range by instruments as LASCO on the *SOHO* spacecraft (left). The big plasma “bubble” thought to make up a CME is likely to be detectable by radars operating in the 10–100 MHz frequency range. Data from *Lang (2000)* [67].

Non-stationary radio emission during periods preceding CME observations has been shown to reflect processes in the lower layers of the solar atmosphere during the period preceding the CME passage into the solar corona [99]. It therefore appears possible to construct algorithms of forecasting CME formation based on radio data [100].

Because CMEs play such a significant role for the state of the Earth’s environment, a thorough understanding of their physics, their initiation and evolution beyond the limits (in wavelength and spatial coverage) of coronagraph images is desirable. The only other point of reference for CME observation is the L1 libration point, about 230 Earth radii in front of the Earth, where in-situ solar wind and magnetic field measurements of the interplanetary medium are continuously taken by space probes such as *Advanced Composition Explorer (ACE)* and *WIND*. Improved monitoring from initial formation through development and modification during their passage through the outer corona and the interplanetary space will aid significantly in understanding CMEs.

3.2.1 The Morphology of Coronal Mass Ejections

Coronal mass ejections (CMEs) constitute a form of intermittent massive expulsion of mass from the solar corona. They may appear with a frequency of one event per every few days during solar minimum to several events per day during solar maximum. They form a bursty type of solar activity and are—if earthward directed—known to be a key causal link between solar events and geomagnetic storms [41, 56].

CMEs were first directly identified in white-light images from a coronagraph flown on *OSO-7* [110] and their rather frequent occurrence has been established through continuous space-borne observations on *OSO-7* [110], *Skylab* [71] and

various subsequent spacecraft such as *Solwind* (P78-1) [77] and *Solar Maximum Mission* (SMM) [70]. The Large Angle and Spectrometric Coronagraph Experiment (LASCO) [18] flown on the *Solar Heliospheric Observatory* (SOHO) [24] which was launched in 1995, has by now provided the most extensive set of CME observations at different optical and near-optical wavelengths during solar conditions ranging from solar minimum to solar maximum. Optical signatures of CME structures have been observed from 1.1 out to 30 solar radii (the inner and outer limits of the LASCO field-of-view).

At solar minimum, the vast majority of CMEs is produced at low solar latitudes, and at solar maximum, at virtually all latitudes in a regime of slow to moderate ambient solar wind speed. At the inner edge of the coronagraph images, CMEs are observed to start at a wide range of velocities, often at a rather low speed of a few tens of km/s, and they frequently undergo acceleration all the way to the outer edge of the coronagraph image [46] up to a velocity of many hundreds of km/s.

The typical CME structure (33% of the cases according to [19]) can be related to the well-known prominence–cavity pattern leading to a three-part configuration: a leading density enhancement, followed by a density depletion, the disconnected coil-shaped flux system supporting the former prominence, again followed by another density enhancement parts of the uplifting prominence. The probable conservation of the magnetic support of the former prominence is the physical key fact for the later identification of in-situ observed magnetic clouds in the solar wind with preexisting CMEs and before existing prominences on the disc.

The other extreme of the CME morphology is a diffuse and structure-less mass cloud (about 25% of the cases). The total mass ejected in one single CME is typically in the 10^{12} to 10^{13} kg range [40]. Plasma temperature and density within CMEs seem to be highly inhomogeneous. There exist early reports on long-standing confinement of cold prominence matter within the CME body. *Woo* [119] presents a density and density inhomogeneity histogram of different coronal structure elements including CMEs.

At large distances from the Sun, plasma density and plasma speed in CMEs are not necessarily different from those of the ambient solar wind. A number of characteristic features including low ion and electron temperatures, counter-streaming suprathermal electrons and energetic ions, higher alpha particle abundance and a strong magnetic field are often found to be associated with CMEs [80].

From solar observations it is evident that the explosive, short time-scale energy release during flares and the long term, gradual energy release expressed by CMEs can be reasonably understood only if both processes are taken as common and probably not independent signatures of a destabilisation of preexisting coronal magnetic field structures. Configurations of several active regions, quiescent prominences and large scale magnetic arcades outside active regions can be source regions of CME formation. The study of formation, acceleration, and propagation of CMEs requires complex observational tools in different spectral ranges at as many “levels” as possible between the photosphere of the Sun and the magnetosphere of the Earth.

3.2.2 CME Probing at Frequencies Outside the Optical Range

An extensive phenomenological knowledge of the optical features of CMEs from about 1.1 to 30 solar radii has been acquired to date, but knowledge beyond those limits is still sparse. Knowledge about CMEs at other than optical wavelengths exists but is very limited. The only detailed investigations which focus on the non-optical range are recent studies of coronal imaging in the soft X-ray regime. *Hudson and Webb* [47] report that the majority (but by far not all) CMEs are associated with soft X-ray flux before and during CME appearance in white light. The X-ray emission regions were typically found to lie asymmetrically underneath the optical CMEs.

Velocity measurements of the solar wind in its acceleration region were carried out in 1984 with Venera orbiters and ground stations using radio sounding techniques [26]. Coronal flow velocities increased from 20 km/s up to 300 km/s for distances from 3 to 20 solar radii. Very recently, passive radio observations of CMEs were performed with the Nançay radio-heliograph at distances around $3R_{\odot}$ [9]. The temporary connection between CMEs and microwave precursors were studied by *Sheiner and Durasova* [98]. They found that the radio precursors lead the CME observations by 20–60 minutes.

Distinct spatial regimes of interest to the understanding of CME physics include the acceleration regime (from the bottom-side corona out to several tens of solar radii) and the interplanetary space. In particular the initiation regime and the physical processes which lead to CME generation and disruption from the corona are poorly understood, probably largely due to the limit (in space and wavelength) on CME observation.

3.2.3 Monitoring CMEs from the Ground

The most detailed CME studies to date have been made from CMEs originating near the solar limb. CMEs originating from regions facing the Earth and from behind the Sun have been observed as well (Halo CMEs) but are less extensively studied due to their poorer visibility in coronagraph images. It is more difficult but nevertheless possible (with the help of the SOHO Extreme Ultraviolet Imaging Telescope, EIT) to distinguish between CMEs propagating toward and away from the Earth. Obviously, only the former can be geoeffective. The NASA *Solar Terrestrial Relations Observatory (STEREO)* mission scheduled for a 2005 launch is expected to provide 3-D coronagraph observations of CMEs (including those which appear as Halo CMEs to an Earth-based observer) supplemented by radio observations in the 1–14 MHz range provided by the WAVES instrument previously used in the *WIND* mission [17]. *STEREO* will thus overcome some of the limits of present-day optical observations. But even if a Halo CME propagates toward the Earth it may still pass by at some distance from the Earth's magnetosphere without affecting geospace. It is therefore insufficient to have CME monitoring constrained to regions close to the Sun if those CMEs which will eventually be geoeffective are to be identified.

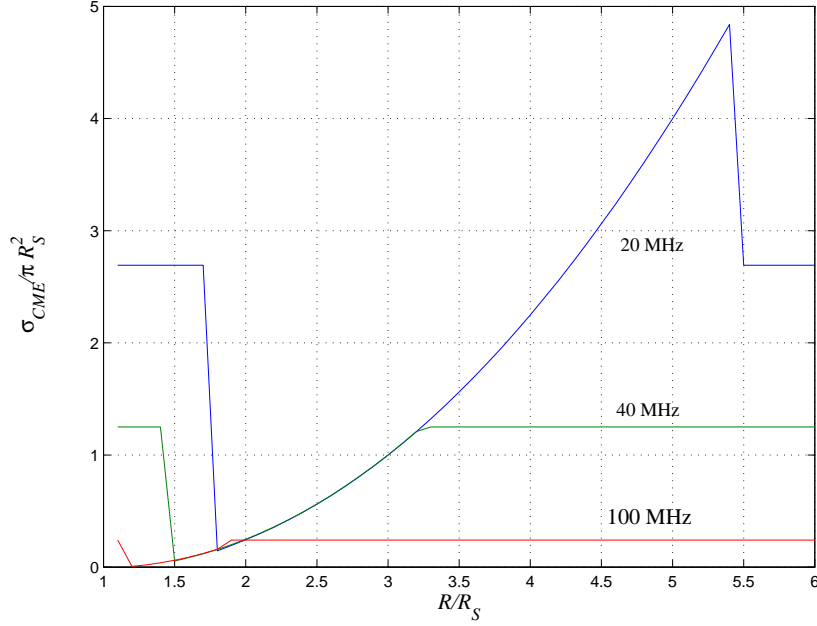


FIGURE 13: Radar cross section for a CME vs. distance R from the CME front to the solar centre for 20 MHz, 40 MHz, and 100 MHz radar frequencies. The CME is assumed to be an expanding spherical plasma shell according to model equation (7).

Radar probing of the solar corona and the interplanetary space with respect to CME evolution and propagation characteristics will thus aid considerably in identifying those CMEs which approach the Earth's magnetosphere.

However, since the successful radar observations of the Sun reported by *Eshleman et al.* [30], *James* [54], and *Campbell and Parrish* [84, 20] at frequencies in the 25–40 MHz range were without any spatial resolution on the Sun, and since no independent solar observations capable of detecting CMEs were made until several years later when CMEs were first discovered, the specific radar signatures of CMEs are not yet known. The radar echoes observed by *James* [54] sometimes exhibited large cross-sections and complex Doppler spectra which are now thought to be related to CMEs.

In order to estimate the expected CME cross-section, we model the CME as an expanding geoeffective plasma shell of radius

$$r = \frac{1}{2}(R - R_{\odot}) \quad (7)$$

The initial plasma density in the CME shell is taken to be 10^{16} m^{-3} [40], in fair agreement with the assumption of a completely ionised proton plasma of mass 10^{12} – 10^{13} kg. The plots in Figures 13 and 14 describe the results.

Radio occultation techniques have been applied to radio signals from various interplanetary space probes when received after passing through the solar corona

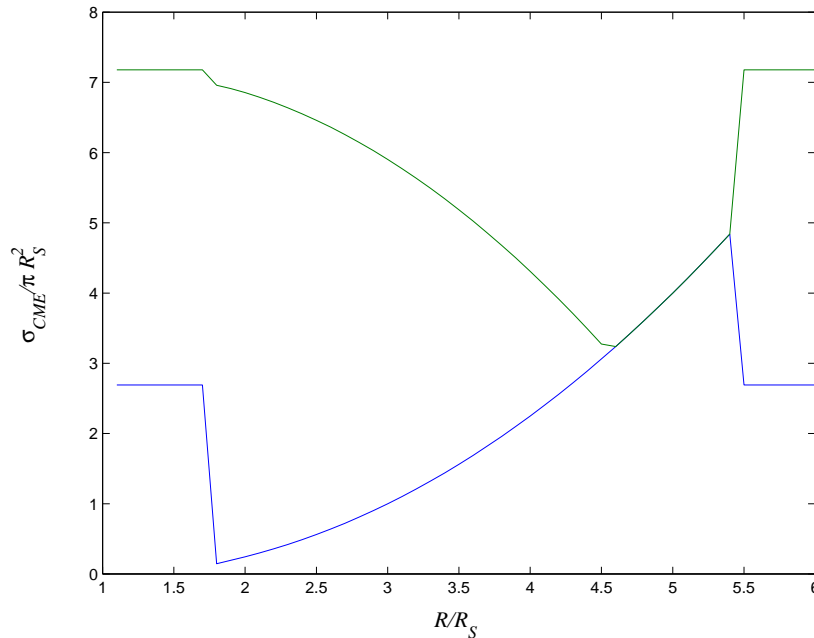


FIGURE 14: Radar cross section for a CME vs. distance R from the CME front to the solar centre for a 20 MHz radar frequency assuming mirror reflection (blue/lower curve) and volume scattering (green/upper curve), respectively. The CME is assumed to be an expanding spherical plasma shell according to model equation (7).

[119]. The fact that CMEs (among other coronal structures) perturb and scatter radio signals has been demonstrated by comparison with simultaneously taken coronagraph images. Intensity scintillations, spectral broadening and Faraday rotation of the radio signals revealed the composite structure of CMEs, in principle a compressed header, a rarefied intermediate region and a high-density body with largely enhanced density fluctuations.

It is likely that the radio perturbation features of CMEs established so far can be exploited by using the LOFAR receiving system in combination with an appropriate transmitter. Radio signals emitted from the Earth would propagate through the front-side corona, be reflected in the middle corona, and return through the front-side corona on their way back to Earth. In order to be successful, the method requires the ability to distinguish between direct solar radiation and backscattered artificial radiation from Earth-based radars. Natural solar radio radiation will increase during solar activity such as bursts, CMEs, *etc.* This might complicate the discrimination of geoeffective CME events against the background solar radiation, but the necessary discrimination may in any case be achieved through the use of coded radar transmissions and advanced polarimetric techniques. It will also be scientifically interesting, and possibly technically necessary, to monitor the natural solar radiation on a separate channel or channels at a frequency or frequencies

close to but different from the radar transmission frequency.

It is interesting to note that the Doppler shift of CMEs propagating along the Sun-Earth line is expected to be of the order of several tens of kHz while the spectral width of the echo may easily be as large as several hundreds of kHz. These estimates are supported by the published data from the El Campo observations. The bandwidths of native solar radio signals are in the MHz range.

Since the characteristics of CME turbulence are not well known, the type of radar backscatter mechanism which may exist is not known either. Various mechanisms were proposed in order to explain the data obtained with the El Campo radar, including turbulence in the local medium [64], fluctuations in the altitude of the plasma resonance level due to electron density fluctuations in the solar wind [50], ion acoustic waves [37] and coherent lower-hybrid waves [118].

If total reflection at the plasma frequency were considered as the main backscatter mechanism, good prospects exist to observe CMEs up to about 2–3 solar radii, according to simulations performed by *Mann et al.* [74]. They arrive at a coronal plasma frequency of around 20 MHz at a distance of 2 solar radii (*cf.* Figure 5).

4 Solar Wind Radar

The solar wind structure has been described in a number of papers and monographs; see *Genkin and Erukhimov* [33] and references cited therein. Our current understanding is that the interplanetary medium is characterized by a large sectorial structure, within which the out-flowing plasma attains speeds, at $R \approx 1$ AU, which are in the range 300–400 km/s under quiet conditions and up to 700–800 km/s in high-speed solar wind streams.

In-situ measurements of solar wind plasma and interplanetary magnetic field made simultaneously by several interplanetary space probes including *ACE*, *WIND*, *Geotail* and *IMP-8*, did not always render consistent results, probably because disturbances in the solar wind can travel in a variety of directions between two extremes: radially away from the Sun (such as the steady solar wind) or guided along the spiral-shaped field lines (such as occasional proton flux bursts). Radar observations of the propagation characteristics of disturbances in the solar wind have the potential of being very useful in augmenting in-situ observations.

Scattering of the radar signals due to shocks, formed, for example, in the interaction between fast and slow solar wind streams, and ahead of CMEs if the speed is high enough; strongly enhanced ion-acoustic turbulence; turbulent structures such as zonal flows [106]; and gradients in the form of plasma bubbles, clouds, plasmoids, *etc.* in interplanetary space, opens up new possibilities of studying the solar wind and the physical mechanism leading to the observed phenomena. As was shown by *Genkin and Erukhimov* [32], a powerful and sensitive radar, operated in the upper HF range, may produce detectable echoes from ion-acoustic turbulence in fast solar wind streams.

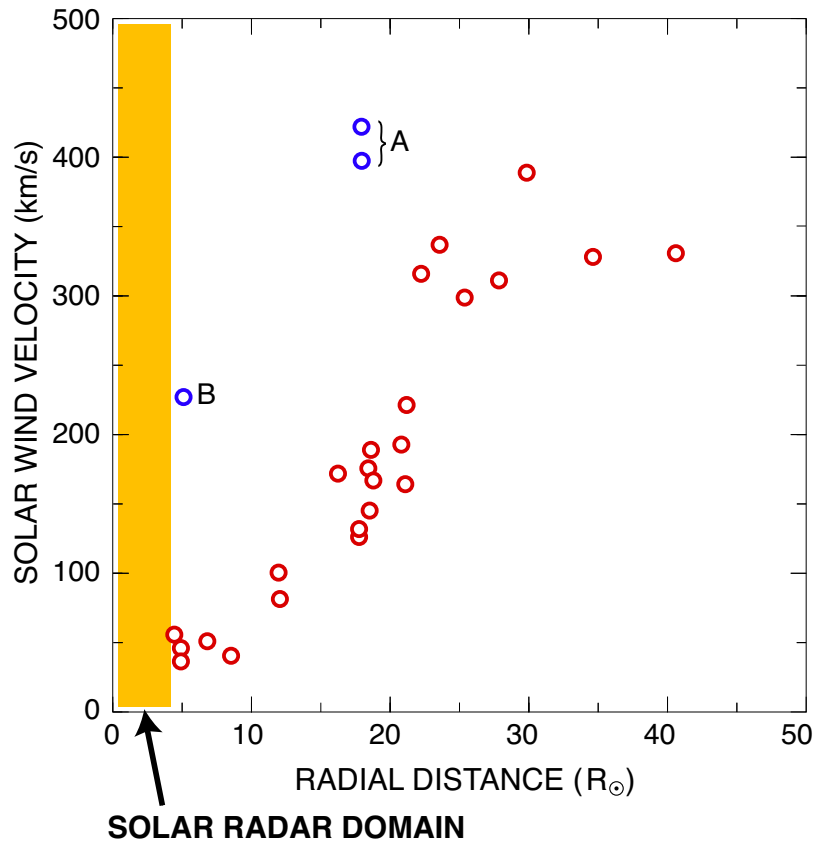


FIGURE 15: The solar wind velocity as a function of radial distance from the Sun obtained from interplanetary scintillation (IPS) measurements made at the Kashima 34-m radio telescope in Japan in 1989. The points indicated by A and B are thought to be related to coronal mass ejection (CME) events. A powerful solar radar would probably allow measurements of the early stages of solar wind acceleration and CME development at low solar altitudes. After Tokomaru *et al.* [108]; see also [109] and [120].

A tentative experimental detection of such turbulence was made in the summer of 1986 with the Sura facility operated at 9 MHz [28]. Echo bursts with a Doppler shift of $f_{\text{Dop}} \approx 19$ kHz, a delay time of $\tau \approx 1.2$ s, and an average scattered signal power of 2×10^{-14} W, were observed. The receiver bandwidth used was 1.5 kHz. The conjectured scattering region was on the day-side at a distance of 33 Earth radii. The solar wind velocity, as determined from f_{Dop} , was estimated at about 400 km/s.

5 High-Altitude Magnetospheric Radar

The solar wind kinetic energy drives several processes in the magnetosphere of the Earth, *e.g.*, convection, current systems and the visual auroral displays. As recently pointed out by *Song and Lysak* [102], a dynamical description of the solar wind-magnetosphere interaction, *e.g.*, by including MHD wave interactions and wave packet dynamics, may lead to a more realistic model of the energy transfer from the solar wind into the magnetosphere; CMEs are believed to cause major magnetospheric storms [104] corresponding to increased solar wind energy input [3]. The increase of energy input rate during CMEs or during other solar wind disturbances will most likely increase the turbulence level at the magnetopause [91].

The energy input rate into the magnetosphere has successfully been described by global parameters [85] suggesting that global dynamics are more important than microscopic transport coefficients in solar wind-magnetosphere coupling. It has been proposed that if certain parameter threshold values be exceeded, in combination with a southward pointing IMF, a substorm to be triggered; Figure 1 in [102] illustrates MHD wave propagation in active magnetospheric regions and that the magnetopause is a highly dynamic region.

With a deep-space radar, we hope to establish the signatures of the bow shock and the magnetopause during a variety of solar wind conditions, including CME encounters, and subsequently to investigate the processes responsible for transferring energy and momentum to the magnetosphere. A primary task would be to establish a relation between the characteristics of the magnetopause as measured by the radar and the energy input rate into the magnetosphere.

The *Cluster* multi-spacecraft mission is now telling us how turbulent these regions are [29]. We see evidence of turbulence, and also of large scale waves (corrugations in the boundary surface). There is also the possibility of diamagnetic structures in these regions, and *Cluster* data appear to show this.

We will search for radar signatures of the auroral acceleration regimes and study their relationship to the energy input rate. We will combine the new data with other information to address issues such as sub-storm triggering loading-unloading, and cause-and-effect relationships. There is reason to assume that multiple acceleration processes may be operative along the field lines at different altitudes [95].

The optical aurora and the auroral oval display great variability, the reason for which is not fully known. Solar wind characteristics, internal magnetospheric conditions, and atmospheric conditions are all suspected of playing a role. We hope to advance the understanding of auroral variability by comparing radar observations of CMEs and radar data characterising the time-dependent solar wind-magnetosphere interaction with characteristic auroral features such as the type of aurora, its intensity, temporal variability, and the size of the auroral oval. In doing so we hope to answer questions such as whether the influence of the solar wind is limited to energy transfer, or whether the signature of a solar wind disturbance has a corresponding signature in the characteristics of the aurora.

6 Low-Altitude Magnetospheric Radar

Space-borne experiments have shown that strong ion-acoustic turbulence can exist on auroral zone magnetic field lines in the magnetosphere at altitudes between 4000 and 13000 kilometres [105, 16, 45]. Radar signals in the upper HF and lower VHF ranges may scatter coherently off this long-Debye-length plasma turbulence so that they can be observed by LOFAR and other high-sensitivity radio telescopes with favourable observing geometries and optimum wavelengths λ_{radar} . Theoretical arguments by *Ginzburg and Rukhadze* [35] suggest that the optimum scattering occurs when $\lambda_{\text{radar}} \approx 5\lambda_{\text{De}}$, which means that a radar frequency of 85 MHz would yield maximum echoes from altitudes around 3000 km; lower frequencies will scatter off magnetospheric ion-acoustic turbulence at higher altitudes.

The first tentative observation of coherent HF radar scattering off magnetospheric ion-acoustic turbulence was made at the Russian Sura facility in 1991 by *Gurevich et al.* [42]. Later, in 1995, scattering off magnetospheric turbulence at about 6000 km was observed in experiments performed at Tromsø where the EISCAT HF facility was operated in a radar mode [107]. The echoes were typically a factor 10^{-20} weaker than the transmitted pulses.

The use of LOFAR along with a separate transmitting facility as a deep-space radar could contribute further to these studies of transient enhancements in back-scattered power from the lower magnetosphere. Incoherent scatter radars have single, point beams, so while they may be used with great accuracy to locate scattering sources in relation to auroral filaments, they will not give a bigger picture—morphology, dynamics, and relation to magnetospheric phenomena—without being operated in (mechanical) scanning mode, which introduces time/space ambiguities into the interpretation of the data.

7 General Remarks

The extension of the LOFAR system to include a radar capability will facilitate a mutually beneficial synergy between astronomy and space physics.

For instance, the study of transient sources in distant Universe will benefit greatly from, and in some cases may not be reliably possible without, an active research programme on the solar-terrestrial relationships discussed here. The knowledge to be developed in this area will thus be important to squeezing the most out of LOFAR itself. An example is variability in local (turbulent) effects, which could hamper a correct interpretation of variable signals.

Likewise, the availability of multi-beaming and high sensitivity during reception could provide discriminatory information important for the correct interpretation of radar signatures. The capability of using many separated beams is something that very few space radars possess.

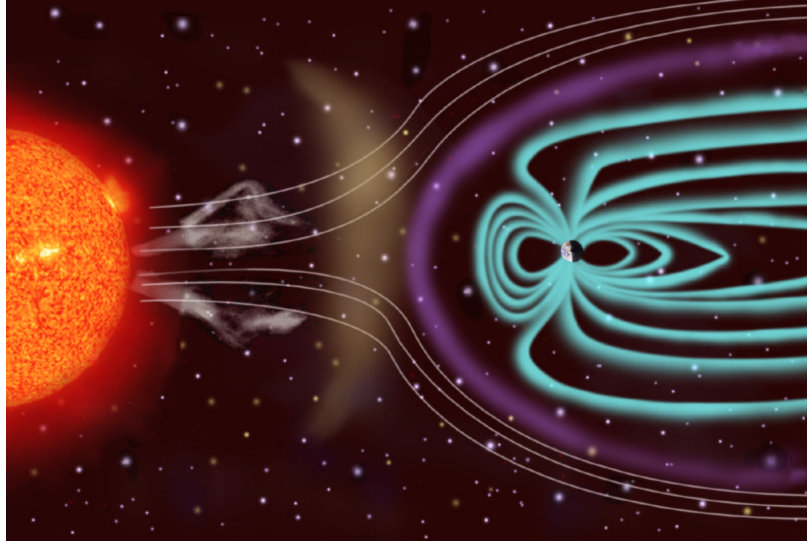


FIGURE 16: The Sun's magnetic field and releases of plasma directly affect Earth and the rest of the solar system. Solar wind shapes the Earth's magnetosphere and magnetic storms are illustrated here as approaching Earth. These storms, which occur frequently, can disrupt communications and navigational equipment, damage satellites, and even cause blackouts. The white lines represent the solar wind; the purple line is the bow shock line; and the blue lines surrounding the Earth represent the magnetosphere.

7.1 Solar Observations

To enhance our knowledge about the solar atmosphere in general, and to overcome the lack in our knowledge about radar signatures of CMEs in particular, we propose to attempt to establish a CME radar signature by using the combination of LOFAR and a radar transmitter sub-facility solar radar measurements taken during limb CMEs which are clearly identified in optical images, *e.g.*, taken with *LASCO* on *SOHO*, will be searched for common radar return characteristics. It may then be possible, by examining radar observations of a large number of optically identified CMEs, to find a characteristic signature in the radar return signals.

Once a sufficiently large “inter-calibration” data base has been assembled, we expect to be in a position to identify and monitor, with the help of solar radar measurements, all CMEs, including those which propagate toward the Earth and are potentially geoeffective. LOFAR and its transmitter will thus assume a role as an important tool for space weather research. For example, there have been reports on strongly geoeffective CMEs which were almost invisible on the solar disk. Dynamically changing faint large scale arcades outside active regions were reported *a posteriori* (*e.g.*, the January 6–11, 1997 CME and the following geomagnetic storm; see *Webb et al.* [115] for a survey). These should be detectable using a LOFAR solar radar system.

LOFAR will also be able to record passive solar radio emissions. Solar type II

radio bursts represent signatures of shock waves in the solar corona [78, 73]. Such shock waves can be driven by fast CMEs if the velocity of the CME exceeds the local Alfvén speed in the solar corona. The relationship between CMEs and solar type II radio bursts is discussed in a review presented by *Aurass* [7]. A statistical study of this relationship has recently been undertaken by *Classen and Aurass* [22]. Thus, the type II burst signature is a nice tracer of coronal shock waves. This information could be essential for active radar measurements of large scale disturbances travelling through the solar corona and therefore radio emission observations should be made concurrently with solar radar observations.

7.2 Magnetospheric Scatter

Ionospheric plasma turbulence, much-studied in recent years in connection with auroral particle precipitation [97], is commonly found around sharp gradients in density, conductivity, *etc.* For example, the edges of the mid-latitude trough can give rise to turbulent structures that lead to coherently enhanced radar scatter. However, we do not know much about underdense radio scattering mechanisms (gradient, Bragg-like irregularities, nonlinear) in the magnetosphere. Hence, we need to investigate experimentally the scatterometric properties of the magnetospheric plasma regions in order to work towards a complete understanding of those mechanisms. This can be addressed by a powerful radar system using LOFAR as a receiver. This topic becomes all the more important in light of the separation arguments which have been made in relation to the four *Cluster* spacecraft. A deep-space radar may be ideal for studying (say) magnetopause and bow shock morphology and dynamics, *e.g.*, large scale waves propagating along the boundary, and oscillations set up in response to a solar wind pressure pulse. As in the ionosphere, we could let spacecraft constellations study small-scale structure, and use radar and optics to paint the bigger picture.

7.3 Radar Scattering Centres of Consequence to Deep-Space Probing

The radar signal on its way to and from targets in deep space may encounter numerous interactions at lower altitudes. In order to correctly interpret the solar and other deep-space echoes, signatures from low-altitude echoes must be identified and subtracted. These signatures, which in themselves will be valuable contributions for the atmospheric and ionospheric scientists, can be caused by, for instance,

- Meteor- and cosmic particle-induced ionisation trails of a transient nature.
- D region turbulence in the altitude range 50–90 km, where the pressure is relatively high, and collision frequencies are greater than the plasma critical frequencies in the layer.

- RF absorption/blackout, which is a major problem at auroral latitudes during disturbed conditions (*e.g.*, substorm onset). This is not such a problem at lower latitudes. Also, nonlinear absorption processes in the D and E regions can result from high power HF waves traversing the ionosphere [63]. However, one can avoid nonlinear absorption by having many small transmitters distributed over a large area and collimate or focus the beams far out in space.
- Sporadic E layers (metal ions). These are a problem mainly at higher latitudes, but mid-latitude sites can also be significantly affected.
- Small-scale F region field-aligned density gradients due to self-organisation. These are known to produce “spread F” traces in ionograms and to be formed in regions illuminated by powerful HF radio waves and thus affect the propagation of other radio waves traversing the same regions.
- Scatter from satellites and man-made space debris. This is not always obvious, nor does it necessarily lead to greatly enhanced power returns. If the cross-section is large, and the scatter is seen through the mean beam then it should be easy to identify. If, however, the scattering cross-section is relatively small, or the satellite is seen through the side-lobes of the antenna, the complications arise. To make it even worse, range aliasing can lead to satellites in geostationary orbit (for example) appearing to orbit at ionospheric altitudes.
- Travelling ionospheric disturbances (or propagating waves in general).
- F region patches. These have recently been suggested to be driven by magnetospheric processes such as magnetic reconnection. Whatever their generation mechanism, the passage of small scale structures through a phased-array HF radar’s (near) field-of-view can lead to aliasing, which is difficult to deal with in routine, automated data reduction.

8 Siting Options

The high- and low-latitude phenomena of HF radio absorption and blackout would lead us to site a low frequency radio astronomy observatory such as LOFAR away from both the auroral zones and magnetic equator in a region with low radio interference levels in the frequency range of interest. As a result, the several LOFAR siting options currently being considered are all located at mid-latitudes. The proposed sites fall broadly into three geographic areas: southwestern Australia, southwestern North America, and northern Europe.

In all cases, a powerful transmitter is required. LOFAR, in turn, is to be optimised for producing aperture synthesis images of objects under observation. Thus

a LOFAR-plus-transmitter combination would form a solar radar system of tremendous potential, significantly more capable than the El Campo system of the 1960s.

However, it is clear that the site choice will influence the possibilities for an appropriate transmitting system for solar and deep-space radar studies using LOFAR. Here we include a brief discussion of proposed sites in Australia, North America, and Europe, and a more in-depth look at two case studies specific to the proposed European site.

8.1 Australia

Of the three regions, southwestern Australia is the most remote, the least-developed, and the most electromagnetically pristine. So far as we are aware, no specific proposal for a transmitter has been made for the Australian site. However, Australia and New Zealand have traditionally hosted strong radio science groups, some of which have already shown interest in the possibility of LOFAR being placed in their neighbourhood. There is thus a reasonable possibility of finding substantial support among local radio, atmospheric, and space physics groups for construction of a suitable transmitter for solar and deep-space radar studies with LOFAR.

8.2 North America

The two locations proposed for LOFAR in the southwestern USA suggest that an existing scientific HF radio transmitter, operated in Alaska by the High Frequency Active Auroral Research Program (HAARP),⁶ might be used in conjunction with LOFAR for solar radar and other active observations. During the summer, the Sun lies about 40 degrees south of the HAARP site, at the extreme edge of the HAARP antenna pointing range, and at that point the Sun would be roughly 40 degrees to the west of LOFAR, thus allowing overlap of the HAARP and LOFAR beams on the Sun. The upper limit of the HAARP transmitter frequency is currently 8 MHz, but plans are in place for upgrading to 10 MHz, the low end of the LOFAR range. Although the 10-MHz frequency is near the limit of what is possible to transmit through the ionosphere, recordings of peak ionospheric F-region frequencies *vs.* time of day and day of year indicate that it may work.

A powerful 26-MHz solar radar system has been informally proposed as an upgrade to the Arecibo Observatory radar in Puerto Rico. With this upgrade in place, Arecibo would operate as a stand-alone solar radar system and would also be fully compatible with the LOFAR receiving system. With LOFAR pointing about 45 degrees west, the two systems would have a bistatic overlap on the Sun of about two hours each day during the northern hemisphere summer. A formal proposal is expected to be made during 2003.⁷

⁶<http://www.haarp.alaska.edu/haarp>

⁷http://www-ece.ucsd.edu/coles/solar_radar

It has been suggested that a new solar radar transmitter should be constructed in Texas, and it is possible that this idea may be developed into a concrete proposal.

8.3 Europe

There is currently an active European project aimed at constructing a high-technology solar radar in southern Sweden. Inspired, in part, by the proposed LOFAR location in the Netherlands and northern Germany, and incorporating the LOFAR name into its own, the LOFAR Outrigger in Scandinavia (LOIS) project⁸ would use advanced radio and computer systems similar to those being considered for LOFAR itself. LOIS will be integrated within the major European initiatives for space weather [68, 69].

The LOIS transmitter will use distributed technology, in which atomic array elements, each transmitting no more than a few kW of power, are phased into groups of roughly 100 to 300 m in size, each of which has the desired transmit beamwidth, but the total power of which is well below the thresholds for creating artificial plasma irregularities in the ionosphere and with correspondingly low side-lobe power levels, thus easily meeting limits for environmental, health, and interference power levels. The radiation from all of the distributed phased groups will be precisely controlled in phase so that, when the signals merge in interplanetary space, the vector **E** and **B** fields of the combined beam are virtually indistinguishable from those produced by an ideal non-distributed transmitter in a vacuum. Like the Arecibo project, LOIS could operate in conjunction with LOFAR or as a stand-alone system. LOIS would be capable of solar radar observations during northern hemisphere summer.

As an example of collaborative studies which might be taken by a LOFAR sub-facility, two case studies focusing on potential collaborations between LOIS and LOFAR with the European Incoherent Scatter Radar (EISCAT) observatory in northern Scandinavia are presented next. This is followed by calculations illustrating a number of global bistatic possibilities for solar radar, with the LOIS transmitter as an example, and receiving sites in several possible locations, including those proposed for the LOFAR system.

8.3.1 Case Study 1: Collaborative Magnetospheric Observations using LOFAR-LOIS and the EISCAT Incoherent Scatter Radars

By combining the auroral zone incoherent scatter radar facilities of the European Incoherent Scatter Scientific Association (EISCAT) with a radar such as the one that would be provided by the proposed LOIS system in combination with LOFAR at the European site, it will be possible to systematically investigate how irregularities along the geomagnetic field line, foot-printed on the EISCAT Tromsø site, scatter the radar signals. Figure 17 depicts the magnetic field line from the Tromsø location, the position of the LOFAR telescope, assumed to be centred on

⁸<http://www.lois-space.org>

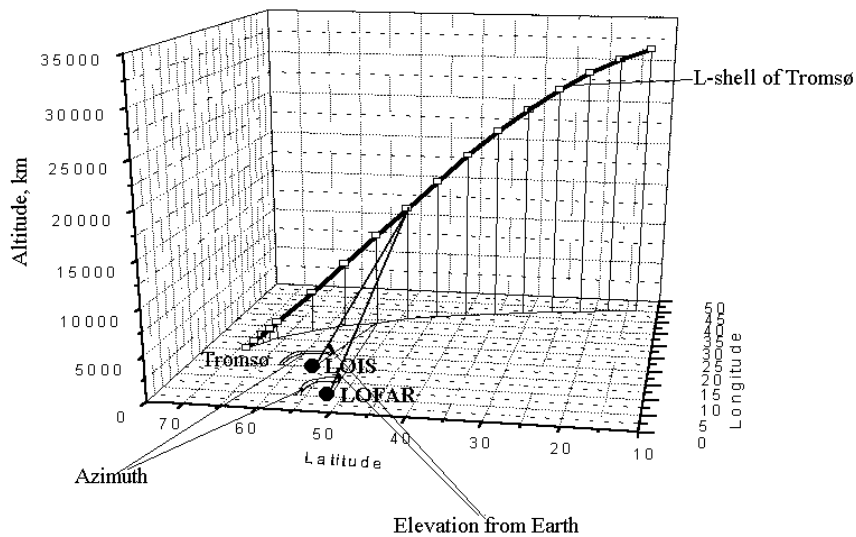


FIGURE 17: The magnetic flux-tube, calculated according to the Tsyganenko model [112], with its footprint at Tromsø. The LOIS and LOFAR sites are depicted, demonstrating that the geometry for radar investigations of the flux tube from these sites is favourable.

Dwingeloo, Netherlands, and the LOIS radar, centred on Växjö, Sweden. Due to the large sizes of the LOIS and LOFAR antenna arrays, the entire magnetosphere will lie in the near fields of both instruments, allowing the possibility of dramatically increasing the power density of the LOIS transmitter, and the sensitivity of the LOFAR receiver, through the use of near-field focusing onto the Tromsø field line. By varying the azimuth and elevation angles, it will be possible to study processes along one and the same magnetic field line over a large altitude range in the magnetosphere. As LOFAR and its supplementary radar facility will be digitally controlled with millisecond agility, varying the pointing, and along with it the focusing, of the two arrays can be done rapidly, thus allowing the separation of temporal and spatial effects.

8.3.2 Case Study 2: Collaborative Studies between LOFAR-LOIS and the EISCAT High-Power HF Transmitter

Recent experiments with the EISCAT high-power, high-frequency (HF) facility outside Tromsø, Norway, have indicated that radio waves from a powerful HF transmitter may cause local activation of aurorae [15]. A mechanism for such an effect has been proposed and is supported by measurements performed with the EISCAT 931-MHz (UHF) radar. The data show that high-power HF radio waves propagating along the direction of the local magnetic field in the night-side au-

roral ionosphere can give rise to a very significant increase in the electron and ion temperatures, T_e and T_i , respectively, along the magnetic field-aligned direction at altitudes up to the upper limit, 600 km, of the measurements. Associated with the increase in T_e and T_i at altitudes above 350 km are intense upward field-aligned ion flows with speeds between 300 and 350 m/s. At the same time, it is believed that heater-induced low-frequency plasma turbulence leads to the formation of field-aligned potential drops, anomalous resistivity, and the generation of parallel electric fields. These fields create an acceleration region at altitudes from 350 to 1000 km, causing the generation of runaway charged particles from the ionosphere.

These effects contribute to the excitation of a turbulent Alfvén boundary layer (TABL) in the ionospheric Alfvén resonator [111, 88, 87]. The excitation of a TABL leads to a decoupling of the magnetospheric convection from the ionospheric drag and triggering of substorms. Still, many questions are outstanding:

- How far out in the magnetosphere do the observed phenomena go?
- What do they produce in the magnetosphere?
- Does a turbulent Alfvén boundary layer really exist? Can it be located in the low-altitude acceleration region?
- What is the role of plasma instabilities in the process?

Supplementing local measurements *in situ* from spacecraft, a sensitive, suitably-located deep-space radar would be an extremely powerful tool to find answers to these and related questions regarding magnetospheric turbulence, ionosphere-magnetosphere coupling, and phenomena initiated by powerful HF radio transmitters.

8.4 Bistatic Radar Geometry

Quite generally, the geometry of an arbitrary bistatic radar setup as illustrated by Figure 18 is characterized by the great circle angle α between the location of the transmitter (TX) and receiver (RX) on the face of the Earth. Assuming Earth to be spherical, α is obtained from the relation

$$\mathbf{X}_{\text{TX}} \cdot \mathbf{X}_{\text{RX}} = |\mathbf{X}_{\text{TX}}| |\mathbf{X}_{\text{RX}}| \cos \alpha \quad (8)$$

where \mathbf{X}_{TX} and \mathbf{X}_{RX} are the vectors from the centre of the Earth to the transmitter and receiver, respectively.

By assuming a geocentric coordinate system and using the latitudinal angles θ_{TX} , θ_{RX} and the longitudinal angles φ_{TX} , φ_{RX} of the transmitter locations and receiver locations, the vectors \mathbf{X}_{TX} and \mathbf{X}_{RX} can be expressed in Cartesian coordinates as

$$\mathbf{X}_{\text{TX}} = (\sin \varphi_{\text{TX}} \cos \theta_{\text{TX}}, \cos \varphi_{\text{TX}} \cos \theta_{\text{TX}}, \sin \theta_{\text{TX}}) R_{\delta} \quad (9)$$

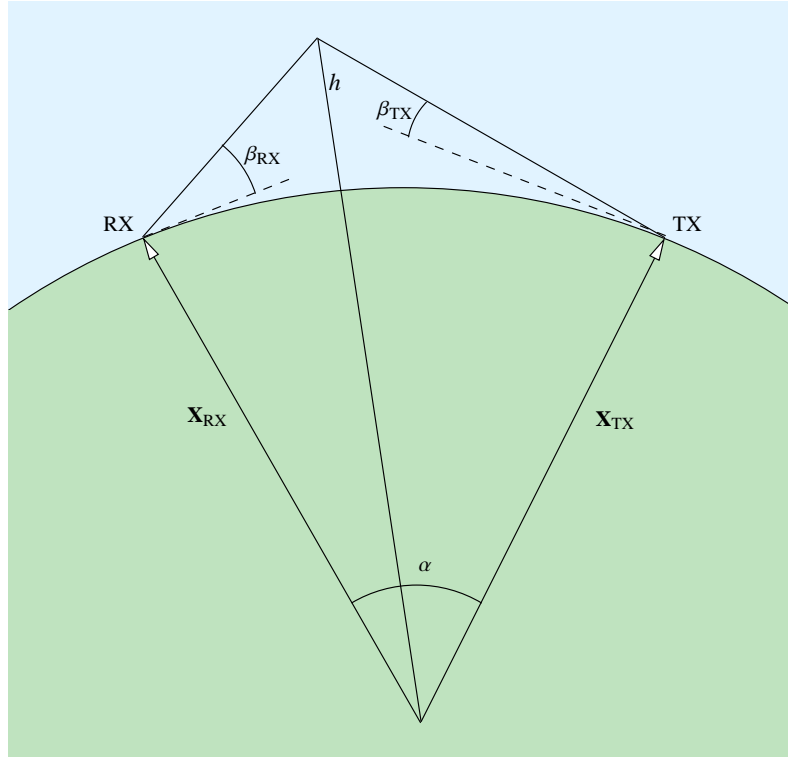


FIGURE 18: The geometry of a bistatic setup with a receiver (RX) and transmitter (TX) located on the surface of the Earth. The height h at which the transmitter and receiver beams intersect is determined by the great circle angle α between the sites and the transmitter and receiver beam elevation angles β_{RX} and β_{TX} , respectively (assuming that the azimuth angles are set so that the beams are along to the great circle).

and

$$\mathbf{X}_{RX} = (\sin \varphi_{RX} \cos \theta_{RX}, \cos \varphi_{RX} \cos \theta_{RX}, \sin \theta_{RX}) R_{\delta} \quad (10)$$

respectively, where the radius of the Earth R_{δ} is approximately 6371 km. From this, one can express the cosine of the great circle angle as

$$\begin{aligned} \cos \alpha = & \sin \varphi_{TX} \cos \theta_{TX} \sin \varphi_{RX} \cos \theta_{RX} \\ & + \cos \varphi_{TX} \cos \theta_{TX} \cos \varphi_{RX} \cos \theta_{RX} + \sin \theta_{TX} \sin \theta_{RX} \end{aligned} \quad (11)$$

Assuming the transmitter to be located in Växjö, Sweden, the great circle angle α to several possible receiving locations has been calculated. The results for receivers at Tremdorf, Germany (Astronomische Institut Potsdam Radioheliograph); Dwingeloo, Netherlands (European LOFAR site); Nançay, France (Observatoire de Paris Radioheliograph); Kharkov, Ukraine (UTR-2 radio telescope); Vasil'sursk, near Nizhniy Novgorod, Russia (Sura radio telescope); Northern Kenya (proposed

TABLE 2: The great circle angle α from a transmitter (TX) at Växjö, Sweden, at 56.8° N, 14.8° E, to several receiving sites (RX) in Europe, Africa, Australia, and North America.

RX	θ_{RX}	φ_{RX}	α
Tremsdorf, Germany	52.3° N	13.1° E	4.6°
Dwingeloo, Netherlands	53.0° N	6.5° E	6.2°
Nançay, France	48.4° N	2.2° E	11.4°
Kharkov, Ukraine	50.0° N	36.2° E	14.3°
Vasil'sursk, Russia	56.2° N	46.0° E	17.0°
Northern Kenya	2° N	37° E	57.5°
Arecibo, Puerto Rico	18.3° N	66.8° W	70.3°
Socorro, New Mexico	34.1° N	107.6° W	77.0°
Western Texas	31° N	104° W	78.3°
Southwestern Australia	30° S	120° E	122.8°

TABLE 3: The heights h of intersecting transmitting beams from Växjö, Sweden (TX), and receiving beams from Dwingeloo, Netherlands (RX), for various transmitter and receiver beam elevation angles β_{TX} and β_{RX} , respectively, and azimuth angles along the TX-RX great circle.

β_{TX}	β_{RX}	h (km)	β_{TX}	β_{RX}	h (km)
0	0	21.0	90	0	84.9
30	30	336	90	30	759
60	60	1069	90	60	2641

Kenya International Radio Observatory, KIRO); Southwestern Australia (Coolgardie, near the proposed Australian LOFAR site); Arecibo, Puerto Rico (Arecibo radar and radio telescope); Socorro, New Mexico, U.S.A. (Very Large Array, one of the two proposed LOFAR sites in the SW USA); and Western Texas, U.S.A. (another proposed North American LOFAR site) are given in Table 2.

For a transmitter in Växjö, Sweden, and a receiver in Dwingeloo, Netherlands, the heights h where the beams cross as a function of different transmitting elevation angles β_{TX} and receiving angles β_{RX} are given in Table 3.

As further illustrated by the two case studies in subsections 8.3.1 and 8.3.2, it is clear that LOIS, in southern Sweden, would work particularly well with LOFAR if LOFAR were constructed in northern Europe. However, as is clear from the bistatic geometry analysis presented above, LOIS could be designed to function as a solar radar system with LOFAR even if LOFAR were located at any one of the other proposed sites. The LOIS site and the proposed North American LOFAR sites are located about 80 degrees apart on a great circle path; however, to intersect

on the Sun, each must steer about 60 degrees off zenith towards a position located over the tropical North Atlantic. The relative pointing would be about the same for the Australian site; if LOFAR were located in southwest Australia, the LOIS and LOFAR beams could intersect on the Sun if each were directed 60 degrees off zenith towards an appropriate point over India. The current LOFAR antenna specifications stipulate that the 3 dB pointing position should be at 60 degrees zenith angle. Thus, if the LOIS antennas were designed to at least match this specification, any of these hypothetical observations would be possible. As with the other potential LOFAR transmitters, all of these solar observations would be performed during northern hemisphere summer.

References

- [1] W. G. ABEL, J. H. CHISHOLM, P. L. FLECK, AND J. C. JAMES, Radar reflections from the Sun at very high frequencies, *J. Geophys. Res.*, 66, 12 (1961), pp. 4303–4307.
- [2] W. G. ABEL, J. H. CHISHOLM, P. L. FLECK, AND J. C. JAMES, A VHF solar radar system, In *IRE Int. Conv. Record*, vol. 10, pt. 5 (1962), pp. 58–66.
- [3] S.-I. AKASOFU, Explosive magnetic reconnection: Puzzle to be solved as the energy supply process for magnetospheric substorms, *EOS*, 66 (1985), p. 9.
- [4] C. E. ALISSANDRAKIS, F. BORGIOLI, F. CHIUDERI DRAGO, M. HAGYARD, AND K. SHIBASAKI, Coronal magnetic fields from microwave polarization observations, *Solar Phys.*, 167 (1996), pp. 167–179.
- [5] C. W. ALLEN, Interpretation of electron densities from corona brightness, *Monthl. Not. Roy. Astr. Soc.*, 107 (1947), pp. 426–432.
- [6] V. I. ALTUNIN, A. F. DEMENT'EV, B. N. LIPATOV, M. V. NECHAEVA, V. A. OKMYANSKIY, S. D. SNEGIREV, AND Y. V. TIKHOMIROV, VLBI studies of the solar-wind plasma irregularities at 18 and 92 cm wavelengths in 1994–1996, *Radiophys. Quant. Electronics*, 43, 3 (2000), pp. 178–186.
- [7] H. AURASS, Coronal mass ejections and type II radio bursts, In *Solar Radiophysics*, G. Trotter, Ed., no. 483 in Lecture Notes in Physics. Springer Verlag, New York, 1997, pp. 136–160.
- [8] F. G. BASS AND S. I. BRAUDE, On the question of reflecting radar signals from the Sun, *Ukrain. J. Phys.*, 2 (1957), pp. 149–163.
- [9] T. S. BASTIAN, M. PICK, A. KERDARON, D. MAIA, AND A. VOURLIDAS, The coronal mass ejection of 1998 April 20: Direct imaging at radio wavelengths, *Astrophys. J.*, 558 (2001), pp. L65–L69.
- [10] S. BAUMBACH, Strahlung, Ergiebigkeit und Elektronendichte der Sonnenkorona, *Astr. Nach.*, 263 (1937), p. 121.
- [11] Y. I. BELOV, S. M. GRACH, AND Y. V. TOKAREV, Unpublished results, private communication, 2002.
- [12] A. O. BENZ AND H. R. FITZE, Microwave radar observations of the Sun, *Astron. Astrophys.*, 76 (1979), pp. 354–355.
- [13] A. O. BENZ AND H. R. FITZE, First solar radar observations in microwaves, In *Radio Physics of the Sun*, M. R. Kundu and T. E. Gergely, Eds. International Astronomical Union, Paris, 1980, pp. 247–250.
- [14] M. K. BIRD, M. PÄTZOLD, P. EDENHOFER, S. W. ASMAR, AND T. P. MCELRATH, Coronal radio sounding with Ulysses: Solar wind electron density near 0.1 AU during the 1995 conjunction, *Astron. Astrophys.*, 316 (1996), pp. 441–448.

- [15] N. F. BLAGOVESHCHENSKAYA, V. A. KORNIENKO, T. D. BORISOVA, B. THIDÉ, M. J. KOSCH, M. T. RIETVELD, E. V. MISHIN, R. Y. LUK'YANOVA, AND O. A. TROSHICHEV, Ionospheric HF pump triggering of local auroral activation, *J. Geophys Res.*, *A12* (2001), pp. 29071–29090.
- [16] R. BOSTRÖM, G. GUSTAFSSON, B. HOLBACK, H. KOSKINEN, AND P. KINTNER, Characteristics of solitary waves and weak double layers in the magnetosphere plasma, *Phys. Rev. Lett.*, *61* (1988), pp. 82–85.
- [17] J.-L. BOUGERET, M. L. KAISER, P. J. KELLOGG, R. MANNING, K. GOETZ, S. J. MONSON, N. MONGE, L. FRIEL, C. A. MEETRE, C. PERCHE, L. SITRUK, AND S. HOANG, WAVES: The radio and plasma wave investigation on the WIND spacecraft, *Space Sci. Rev.*, *71* (1995), pp. 231–263.
- [18] G. E. BRUECKNER, R. A. HOWARD, M. J. KOOMEN, C. M. KORENDYKE, D. J. MICHELS, J. D. MOSES, D. S. SOCKER, K. P. DERE, P. L. LAMY, A. LLEBERIA, M. V. BOUT, R. SCHWENN, G. M. SIMNETT, D. K. BEDFORD, AND C. J. EYLES, The Large Angle Spectroscopic Coronagraph (LASCO), *Solar Phys.*, *162* (1995), pp. 357–402.
- [19] J. BURKEPILE AND O. C. ST. CYR, A revised and expanded catalogue of mass ejections observed by the Solar Maximum Mission coronagraph, NCAR/TN 369+STR, National Center for Atmospheric Research, Boulder, CO, Jan. 1993.
- [20] D. CAMPBELL, Private communication, 1998.
- [21] J. H. CHISHOLM AND J. C. JAMES, Radar evidence of solar wind and coronal mass motions, *Astrophys. J.*, *140* (1964), pp. 377–379.
- [22] H.-T. CLASSEN AND H. AURASS, On the association between type II radio bursts and CMEs, *Astron. Astrophys.*, *384* (2002), pp. 1098–1106.
- [23] K. DAVIES, *Ionospheric Radio*, No. 31 in IEE Electromagnetic Waves Series. Peter Peregrinus Ltd., Stevenage, Herts., UK, 1990.
- [24] V. DOMINGO, B. FLECK, AND A. I. POLAND, The SOHO mission: An overview, *Solar Phys.*, *162* (1995), pp. 1–37.
- [25] C. DYBAS, Scientists to present results of “solar storm” research—massive events disrupt power, cause aurora displays, National Science Foundation Press Release 96-20, 8 May 1996.
- [26] A. I. EFIMOV, Radial profile measurements of the solar wind speed using radio sounding techniques, *Space Sci. Rev.*, *70/1-2* (1994), pp. 397–402.
- [27] W. C. ERICKSON, The radio wave scattering properties of the solar corona, *Astrophys. J.*, *139* (1964), pp. 1290–1311.
- [28] L. M. ERUKHIMOV, Private communication, 1993.
- [29] P. ESCOUBET, Ed., *Annales Geophysicae, Special Issue: CLUSTER – First Results (Part I)*, vol. 19, European Geophysical Society, October/December 2001, pp. 1195–1449.

- [30] V. R. ESHLEMAN, R. C. BARTHLE, AND P. B. GALLAGHER, Radar echoes from the Sun: Man's first contact with the sun opens new approaches for the study of solar events, *Science*, 131 (1960), pp. 329–332.
- [31] H. R. FITZE AND A. O. BENZ, The microwave solar radar experiment, I, Observations, *Astrophys. J.*, 250 (1981), pp. 782–790.
- [32] L. G. GENKIN AND L. M. ERUKHIMOV, The possibilities of measuring the ionosonic turbulence of the interplanetary plasma and the solar wind velocity by the radiowave back-scattering method, *Geom. Aeron.*, 23 (1983), pp. 324–326.
- [33] L. G. GENKIN AND L. M. ERUKHIMOV, Interplanetary plasma irregularities and ion acoustic turbulence, *Phys. Rep.*, 183 (1990), pp. 97–148.
- [34] V. L. GINZBURG, *The Propagation of Electromagnetic Waves in Plasmas*, second, revised and enlarged ed., Pergamon Press, Oxford, 1970.
- [35] V. L. GINZBURG AND A. A. RUKHADZE, *Waves in magnetized plasma*, Nauka, Moscow, 1975.
- [36] W. D. GONZALEZ AND B. T. TSURUTANI, Criteria of interplanetary parameters causing intense magnetic storms ($D_{st} < -100$ nT), *Planet. Space Sci.*, 35 (1987), pp. 1101–1109.
- [37] I. M. GORDON, Interpretation of radio echoes from the Sun, *Astrophys. Lett.*, 2 (1968), pp. 49–53.
- [38] I. M. GORDON, Radar observations of the sun, and a mechanism for producing the reflected signal in the corona, *Astronomicheskii Zhurnal*, 45 (1968), pp. 1002–, (for Engl. transl. see Soviet Astronomy, 12, 796-, 1969).
- [39] I. M. GORDON, Plasma theory of radio echoes from the sun and its implication for the problem of the solar wind, *Space Sci. Rev.*, 15 (1973), pp. 157–204.
- [40] J. T. GOSLING, Coronal mass ejections: An overview, In *Coronal Mass Ejections*, J. J. Nancy Crooker and J. Feynman, Eds., Geophysical Monograph 99. American Geophysical Union, Washington DC, 1997, pp. 9–16.
- [41] J. T. GOSLING, D. J. MCCOMAS, J. L. PHILLIPS, AND S. J. BAME, Geomagnetic activity associated with earth passage of interplanetary shock disturbances and coronal mass ejections, *J. Geophys. Res.*, 96, A5 (1991), pp. 7831–7839.
- [42] A. V. GUREVICH, A. M. BABICHENKO, A. N. KARASHTIN, AND V. O. RAPOPORT, HF sounding of the auroral magnetosphere, *J. Geophys. Res.*, 97, A6 (1992), pp. 8693–8696, (In Russian: Pis'ma ZhETF, 53, (1991), pp. 139–143).
- [43] W. HANLE, Über magnetische Beeinflussung der Polarisation der Resonanzfluoreszenz, *Z. Phys.*, 30 (1924), pp. 93–105.
- [44] J. S. HEY, Solar radiation in the 4–6 metre radio wave-length band, *Nature*, 157 (1946), pp. 47–48.

- [45] G. HOLMGREN AND P. M. KINTNER, Experimental evidence of widespread regions of small-scale plasma irregularities in the magnetosphere, *J. Geophys. Res.*, 95 (1990), pp. 6015–6023.
- [46] R. A. HOWARD, G. E. BRUECKNER, O. C. ST. CYR, D. A. BIESECKER, K. P. DERE, M. J. KOOMEN, C. M. KORENDYKE, P. L. LAMY, A. LLEBARIA, M. V. BOUT, D. J. MICHELS, J. D. MOSES, S. E. PASWATERS, S. P. PLUNKETT, R. SCHWENN, G. M. SIMNETT, D. G. SOCKER, S. J. TAPPIN, AND D. WANG, Observations of CMEs from SOHO/LASCO, In *Coronal Mass Ejections*, J. J. Nancy Crooker and J. Feynman, Eds., Geophysical Monograph 99. American Geophysical Union, Washington DC, 1997, pp. 17–26.
- [47] H. S. HUDSON AND D. F. WEBB, Soft X-ray signatures of coronal ejections, In *Coronal Mass Ejections*, J. J. Nancy Crooker and J. Feynman, Eds., Geophysical Monograph 99. American Geophysical Union, Washington DC, 1997, pp. 27–38.
- [48] A. J. HUNDHAUSEN, *Coronal expansion and solar wind*, Springer-Verlag, New York, 1972.
- [49] R. D. HUNSUCKER, *Radio Techniques for Probing the Terrestrial Ionosphere*, No. 22 in Physics and Chemistry in Space. Springer-Verlag, New York, 1991, ISBN 0-387-53406-7.
- [50] A. ISHIMARU AND R. WOO, Interpretation of radar measurements of the Sun, *EOS*, 59 (1978), p. 1175.
- [51] J. C. JAMES, Radar echoes from the sun, *IEEE Trans. Mil. Elect.*, MIL-8 (July–October 1964), pp. 210–225, Identical to *IEEE Trans. Antennas Propagat.*, AP-12, 876–891.
- [52] J. C. JAMES, A 38 Mcps solar radar system, *NEREM Record*, 7 (1965), pp. 186–187, [Northeast Electronics Research and Engineering Meeting, Session: Radar Astronomy, FAM-1, Fri, 5 Nov 1965].
- [53] J. C. JAMES, Radar studies of the sun at 38 Mc/s, *Astrophys. J.*, 146 (1966), pp. 356–366.
- [54] J. C. JAMES, Radar studies of the sun, In *Radar Astronomy*, J. V. Evans and T. Hagfors, Eds. McGraw-Hill Book Co., New York, 1968, Library of Congress Catalog Card Number 66-29751.
- [55] J. C. JAMES, Some observed characteristics of solar radar echoes and their implications, *Solar Phys.*, 12 (1970), pp. 143–151.
- [56] S. W. KAHLER, Solar flares and coronal mass ejections, *Ann. Rev. Astron. Astrophys.*, 30 (1992), pp. 113–141.
- [57] A. KARASHTIN, V. FRIDMAN, AND O. SHEINER, Private communication, 2002.
- [58] A. N. KARASHTIN, G. P. KOMRAKOV, Y. V. TOKAREV, AND Y. V. SHLUGAEV, Solar monostatic radio sounding at the SURA facility, In *VII Russian-UIS Symposium on Solar-Terrestrial Physics, Book of Abstracts* (Moscow, Dec 15-18, 1998), pp. 24–25.

- [59] A. N. KARASHTIN, G. P. KOMRAKOV, Y. V. TOKAREV, AND Y. V. SHLYUGAEV, Radar studies using the SURA facility, *Radiophys. Quant. Electronics*, *42*, 8 (1999), pp. 674–686.
- [60] F. J. KERR, On the possibility of obtaining radar echoes from the Sun and the planets, *Proc. IRE*, *40* (1952), pp. 660–666.
- [61] F. J. KERR, Radio echoes from the Sun, Moon, and the planets, In *Handbuch der Physik*, vol. LII. Springer-Verlag, Berlin, 1959, pp. 449–464.
- [62] H. KOHL, R. RÜSTER, AND K. SCHLEGEL, Eds., *Modern Ionospheric Science, A Collection of Articles published on the Occasion of the Anniversary: “50 years of Ionospheric Research in Lindau”*, European Geophysical Society, Katlenburg-Lindau, 1996, ISBN 3-9804862-1-4.
- [63] D. S. KOTIK AND M. A. ITKINA, On the physical limit of the power of heating facilities, *J. Atmos. Sol.-Terr. Phys.*, *60* (1998), pp. 1247–1256.
- [64] M. R. KUNDU, *Solar Radio Astronomy*, vol. 52, Interscience Publishers, New York, 1965, Ch. 17.
- [65] K. R. LANG, *Astrophysical Formulae*, Springer-Verlag, Berlin, 1980, Eqns. (3-279) and (3-280).
- [66] K. R. LANG, *Sun, Earth and Sky*, Springer-Verlag, Berlin, 1995, ISBN 3-540-58778-0.
- [67] K. R. LANG, *The Sun from Space*, Springer-Verlag, Berlin, 2000.
- [68] H. LUNDSTEDT, The Swedish space weather initiatives, In *Proceedings of Workshop on Space Weather* (Noordwijk, The Netherlands, 11–13 November 1998), ESA WPP-155, ESTEC, pp. 197–205.
- [69] H. LUNDSTEDT, Forecasting space weather and effects using knowledge-based neurocomputing, In *Proceedings of Space Weather Workshop* (Noordwijk, The Netherlands, 17–19 December 2001), ESTEC.
- [70] R. M. MACQUEEN, A. CSOEKE-POECKE, E. HILDNER, R. REYNOLDS, A. STANGER, H. TE POEL, AND W. J. WAGNER, The High Altitude Observatory coronagraph/polarimeter on the Solar Maximum Mission, *Solar Phys.*, *65* (1980), pp. 91–107.
- [71] R. M. MACQUEEN, J. A. EDDY, J. T. GOSLING, E. HILDNER, R. H. MUNRO, G. A. NEWKIRK, A. I. POLAND, AND C. L. ROSS, The outer corona as observed from Skylab, *Astrophys. J. Lett.*, *187* (1974), pp. L85–L88.
- [72] S. MANCUSO AND S. R. SPANGLER, Faraday rotation and models for the plasma structure of the solar corona, *Astrophys. J.*, *539* (2000), pp. 480–491.
- [73] G. MANN, Theory and observations of coronal shock waves, In *Coronal Magnetic Energy Releases*, A. O. Benz and A. Krüger, Eds., Lecture Notes in Physics. Springer Verlag, New York, 1995, p. 183.

- [74] G. MANN, F. JENSEN, R. J. MACDOWALL, M. L. KAISER, AND R. G. STONE, A heliospheric density model and type III radio bursts, *Astron Astrophys.*, 348 (1999), pp. 614–620.
- [75] G. MANN, H. O. RUCKER, AND J.-L. BOUGERET, Solar encounter—the first solar orbiter workshop, *ESA-SP493* (2001), p. 289.
- [76] A. H. MCALLISTER AND N. U. CROOKER, Coronal mass ejections, co-rotating interaction regions, and geomagnetic storms, In *Coronal Mass Ejections*, J. J. Nancy Crooker and J. Feynman, Eds., Geophysical Monograph 99. American Geophysical Union, Washington DC, 1997, pp. 279–289.
- [77] D. J. MICHELS, R. A. HOWARD, M. J. KOOMEN, AND J. N. R. SHEELEY, Satellite observations of the outer corona near sunspot maximum, In *Radio Physics of the Sun*, M. R. Kundu and T. E. Gergely, Eds. D. Reidel Publ. Co., Hingham, MA, 1980, p. 439.
- [78] G. S. NELSON AND D. MELROSE, Type II bursts, In *Solar Radiophysics*, D. J. McLean and N. R. Labrum, Eds. Cambridge University Press, New York, 1985, p. 333.
- [79] M. NEUGEBAUER AND R. GOLDSTEIN, CMEs and space weather, In *Coronal Mass Ejections*, J. J. Nancy Crooker and J. Feynman, Eds., Geophysical Monograph 99. American Geophysical Union, Washington DC, 1997, pp. 291–299.
- [80] M. NEUGEBAUER AND R. GOLDSTEIN, Particle and field signatures of coronal mass ejections in the solar wind, In *Coronal Mass Ejections*, J. J. Nancy Crooker and J. Feynman, Eds., Geophysical Monograph 99. American Geophysical Union, Washington DC, 1997, pp. 245–251.
- [81] G. NEWKIRK, JR., The solar corona in active regions and the thermal origin of the slowly varying component of solar radio radiation, *Astrophys. J.*, 133 (1961), pp. 983–1013.
- [82] S. J. OSTRO, Planetary radar astronomy, *Rev. Mod. Phys.*, 65 (1993), pp. 1235–1279.
- [83] E. N. PARKER, *Interplanetary Dynamical Processes*, Wiley, New York, 1963.
- [84] A. PARRISH, Solar radar experiments, 1967, Tech. Rep. 300, Center for Radiophysics and Space Research, Cornell University, Ithaca, New York, April 1968.
- [85] P. PERREAULT AND S.-I. AKASOFU, A study of magnetic storms, *Geophys. J. R. Astron. Soc.*, 54 (1978), p. 547.
- [86] J. L. PHILLIPS, S. J. BAME, A. BARNES, B. L. BARRACLOUGH, W. C. FELDMAN, B. E. GOLDSTEIN, J. T. GOSLING, G. W. HOOGEVEEN, D. J. MCCOMAS, M. NEUGEBAUER, AND S. T. SUESS, Ulysses solar wind plasma observations from pole to pole, *Geophys. Res. Lett.*, 22 (1995), pp. 3301–3304.
- [87] O. A. POKHOTILOV, V. KHRUSCHEV, M. PARROT, S. SENCHENKOV, AND V. P. PAVLENKO, Ionospheric Alfvén resonator revisited: Feedback instability, *J. Geophys. Res.*, 106, A12 (2001), pp. 7491–7508.

- [88] O. A. POKHOTELOV, D. POKHOTELOV, V. STRELTSOV, V. KHRUSCHEV, AND M. PARROT, Dispersive ionospheric resonator, *J. Geophys. Res.*, *105*, A4 (2000), p. 7737.
- [89] E. R. PRIEST, *Solar Magnetohydrodynamics*, Reidel, 1982.
- [90] M. PÄTZOLD, M. K. BIRD, H. VOLLAND, G. S. LEVY, B. L. SEIDEL, AND C. T. STELZRIED, The meand coronal magnetic field determined from *Helios* Faraday rotation measurements, *Solar Phys.*, *109* (1987), pp. 91–105.
- [91] L. REZEAU AND G. BELMONT, Magnetic turbulence at the magnetopause, a key problem for understanding solar wind/magnetosphere exchanges, *Space Sci. Rev.*, *95/1-2* (2001), pp. 427–441.
- [92] P. RODRIGUEZ, High frequency radar detection of coronal mass ejections, In *Solar Drivers of Interplanetary and Terrestrial Disturbances*, K. S. Balasubramaniam, S. L. Kiel, and R. N. Smartt, Eds., vol. Conference Series 95. Astronomical Society of the Pacific (ASP), 1996, pp. 180–188.
- [93] P. RODRIGUEZ, Radar studies of the solar corona: A review of experiments using HF wavelengths, In *Radio Astronomy at Long Wavelengths*, K. S. Balasubramaniam, S. L. Kiel, and R. N. Smartt, Eds., vol. Geophysical Monograph 119. American Geophysical Union, 2000, pp. 155–165.
- [94] P. RODRIGUEZ, A. KONOVALENKO, O. ULYANOV, L. M. ERUKHIMOV, Y. BELOV, Y. TOKAREV, A. KARASHTIN, AND K. VAN'T KLOOSTER, Detection of HF radar reflection from the solar corona, In *Transactions of the AGU, EOS Supplemental Issue*, vol. 78. American Geophysical Union, 1997, p. F538, (Paper SH21A-15, AGU Fall Meeting, San Fransisco, CA, December 8–12, 1997).
- [95] E. SAGAWA, I. IWAMOTO, S. WATANABE, B. A. WHALEN, AND A. W. YAU, Low energy upflowing ion events observed by EXOS-D: Initial results, *Geophys. Res. Lett.*, *18*, 2 (1991), pp. 337–340.
- [96] R. SCHWENN AND E. MARSCH, *Physics of the Inner Heliosphere*, vol. 1, Large-Scale Phenomena, Springer-Verlag, Berlin, Heidelberg, New York, 1990, ISBN 3-540-52081-3.
- [97] F. SEDGEMORE-SCHULTHESS AND J.-P. ST.-MAURICE, Naturally enhanced ion-acoustic spectra and their interpretation, *Surveys Geophys.*, *22* (2001), pp. 55–92.
- [98] O. A. SHEINER AND M. S. DURASOVA, Solar microwave precursors and coronal mass ejection—possible connection, *Radiophys. Quant. Electronics*, *37* (1995), pp. 575–578.
- [99] O. A. SHEINER, M. S. DURASOVA, AND V. M. FRIDMAN, The precursors of CME onset in solar radio emission, In *Proceedings of the 9th European Meeting on Solar Physics Magnetic Fields and Solar Processes* (Florence, Italy, 12–18 September 1999), ESA SP-448, European Space Agency, pp. 979–982, ISBN 92-9092-792-5.

- [100] O. A. SHEINER, V. M. FRIDMAN, AND M. S. DURASOVA, Characteristics of nonstationary solar radio emission corresponding to CME formation in the solar atmosphere, In *Proceedings of the SOLSPA 2001 Euroconference: Solar Cycle and Space Weather* (Vico Equense, Italy, 2001), ESA SP-447, European Space Agency.
- [101] P. SONG, H. J. SINGER, AND G. L. SISCOE, Eds., *Space Weather*, Geophysical Monograph 125. American Geophysical Union, Washington DC, 2001.
- [102] Y. SONG AND R. L. LYSAK, Towards a new paradigm: From a quasi-steady description to a dynamical description of the magnetopause, *Space Sci. Rev.*, 95/1-2 (2001), pp. 273–292.
- [103] G. J. SOUTHWORTH, Microwave radiation from the Sun, *J. Franklin. Inst.*, 239 (1945), pp. 285–297.
- [104] Z. ŠVETSKA, Varieties of coronal mass ejections and their relation to flares, *Space Sci. Rev.*, 95/1-2 (2001), pp. 135–146.
- [105] M. TEMERIN, K. CERNY, W. LOTKO, AND F. S. MOZER, Observations of double layers and solitary waves in the auroral plasma, *Phys. Rev. Lett.*, 48 (1982), pp. 1175–1179.
- [106] P. W. TERRY, Suppression of turbulence and transport by sheared flow, *Rev. Mod. Phys.*, 72 (2000), pp. 109–165.
- [107] B. THIDÉ, T. CAROZZI, AND M. RIETVELD, Unpublished results, 1995.
- [108] M. TOKUMARU, H. MORI, T. TANAKA, T. KONDO, H. TAKABA, AND Y. KOYAMA, Solar wind near the Sun observed with interplanetary scintillation using three microwave frequencies, *J. Geomagn. Geoelectr.*, 43 (1991), p. 619.
- [109] M. TOKUMARU, H. MORI, T. TANAKA, T. KONDO, H. TAKABA, AND Y. KOYAMA, Solar wind motion near the Sun derived from simultaneous interplanetary scintillation observations at 2 GHz and 8 GHz, *J. Geomagn. Geoelectr.*, 46 (1994), p. 835.
- [110] R. TOUSEY, The solar corona, In *Space Research XIII*, M. J. Rycroft and S. K. Runcorn, Eds. Akademie-Verlag, Berlin, 1973, pp. 713–730.
- [111] V. Y. TRAKHTENGERTS, P. P. BELYAEV, S. V. POLYAKOV, A. G. DEMEKHOV, AND T. BÖSINGER, Excitation of Alfvén waves and vortices in the ionospheric Alfvén resonator by modulated powerful radiowaves, *J. Atmos. Sol.-Terr. Phys.*, 62 (2000), pp. 267–276.
- [112] N. A. TSYGANENKO, Quantitative models of the magnetospheric magnetic field: Methods and results, *Space Sci. Rev.*, 54/1+2 (1989), pp. 75–186.
- [113] G. L. TYLER, J. P. BRENKLE, T. A. KOMAREK, AND A. I. ZYGIELBAUM, The viking solar corona experiment, *J. Geophys. Res.*, 82, 28 (1977), pp. 4335–4340.
- [114] A. VÄSTBERG, *Investigation of the Ionospheric HF Channel by Ray Tracing*, PhD thesis, Uppsala University, Uppsala, Sweden, Apr. 1997, IRF Sci. Rep., 241.

- [115] D. F. WEBB, E. W. CLIVER, N. U. CROOKER, O. C. ST. CYR, AND B. J. THOMPSON, Relationship of halo coronal mass ejections, magnetic clouds, and magnetic storms, *J. Geophys. Res.*, *105*, A2 (2000), pp. 7491–7508.
- [116] D. F. WEBB, J. C. JOHNSTON, AND R. R. RADICK, The Solar Mass Ejection Imager (SMEI): A new tool for space weather, *EOS, Trans. AGU*, *83* (2002), pp. 33,38–39.
- [117] J. M. WEISBERG, J. M. RANKIN, R. R. PAYNE, AND C. C. COUNSELMANN, Further changes in the distribution of density and radio scattering in the solar corona in 1973, *Astrophys. J.*, *209* (1976), pp. 252–258.
- [118] D. G. WENTZEL, A new interpretation of James's solar radar echoes involving lower-hybrid waves, *Astrophys. J.*, *248* (1981), pp. 1132–1143.
- [119] R. WOO, Mass ejections observed in radio propagation measurements through the solar corona, In *Coronal Mass Ejections*, J. J. Nancy Crooker and J. Feynman, Eds., Geophysical Monograph 99. American Geophysical Union, Washington DC, 1997, pp. 235–244.
- [120] Y. YAMAUCHI, M. TOKUMARU, M. KOJIMA, P. K. MANOHARAN, AND R. ESSER, A study of density fluctuations in the solar wind acceleration region, *J. Geophys. Res.*, *103*, A4 (1998), pp. 6571–6583.
- [121] V. V. ZHELEZNYAKOV, *Radio Emission of the Sun and the Planets*, Pergamon Press, Oxford, 1970.

